

# **Combined impacts of climate change and human activities on blue and green water resources in the high-intensity development watershed**

Xuejin Tan<sup>1</sup>, Bingjun Liu<sup>2\*</sup>, Xuezhi Tan<sup>2,3\*</sup>, Zeqin Huang<sup>2</sup>, Jianyu Fu<sup>2</sup>

<sup>1</sup> School of Geography and Planning, Sun Yat-sen University, Guangzhou, 510006, PR China

<sup>2</sup> Center of Water Resources and Environment, School of Civil Engineering, Sun Yat-sen University, Guangzhou, 510275, PR China

<sup>3</sup> Southern Marine Science and Engineering Guangdong Laboratory (Zhuhai), Sun Yat-sen University, Zhuhai, 519082, PR China

\* Corresponding authors: Bingjun Liu ([liubj@mail.sysu.edu.cn](mailto:liubj@mail.sysu.edu.cn))

Xuezhi Tan ([tanxuezhi@mail.sysu.edu.cn](mailto:tanxuezhi@mail.sysu.edu.cn))

## 1 Abstract

2 Sustainable management of blue and green water resources is vital for the stability and  
3 sustainability of watershed ecosystems. Although there has been extensive attention to blue water  
4 (*BW*) which is closely related to human beings, the relevance of green water (*GW*) for ecosystem  
5 security is typically disregarded in water resource evaluations. Specifically, comprehensive studies  
6 are scarce on the detection and attribution of variations of blue and green water in the Dongjiang  
7 River Basin (DRB), an important source of regional water supply in the Guangdong-Hong Kong-  
8 Macao Greater Bay Area (GBA) of China. Here we assess the variations of *BW* and *GW* scarcity,  
9 and quantify the impacts of climate change and land use change on *BW* and *GW* in DRB using a  
10 multi-water-flux calibrated Soil and Water Assessment Tool (SWAT). Results show that *BW* and  
11 green water storage (*GWS*) in DRB increased slowly with a rate of 0.14 and 0.015 mm a<sup>-1</sup>,  
12 respectively, while green water flow (*GWF*) decreased significantly at a rate of -0.21 mm a<sup>-1</sup>. The  
13 degree of *BW* and *GW* scarcity in DRB is low, and the per capita water resources in more than 80%  
14 of DRB exceed 1700 m<sup>3</sup> capita<sup>-1</sup> a<sup>-1</sup>. Attribution results show that 88.0%, 88.5%, and 39.4% of  
15 changes in *BW*, *GWF*, and *GWS* result from climate change, respectively. Both climate change and  
16 land use change have decreased *BW*, while climate change (land use change) ~~have~~has decreased  
17 (increased) *GWF* in DRB. These findings can guide the optimization of the allocation of blue and  
18 green water resources between upper and lower reach areas in DRB and further improve the  
19 understanding of blue and green water evolution patterns in humid regions.

20 **Key words:** Blue and green water; Water scarcity; Climate change, Land use change; Water flow;  
21 Dongjiang River Basin

## 22 1 Introduction

23 Land use and land cover change (LUCC), and climate variability may alter hydrological

24 processes in watersheds (Berezovskaya et al., 2004; Chagas et al., 2022; Konapala et al., 2020;  
25 Tan et al., 2022a), which successively affect variations of regional water resources (Hoek van  
26 Dijke et al., 2022; Pokhrel et al., 2021; Stocker et al., 2023; Suzuki et al., 2021), potentially leading  
27 to ecosystem degradation and severe water shortage crises (Aghakhani Afshar et al., 2018; Zuo et  
28 al., 2015). With the development of society and the economy, there is an increasing need of water  
29 resources to accommodate human water utilization, encompassing agricultural, domestic, and  
30 industrial water usage. Water scarcity and spatiotemporal mismatch between regional water supply  
31 and demand in certain regions are becoming increasingly severe, significantly affecting sustainable  
32 development in these regions (Cook et al., 2014). Quantifying water resources in a changing  
33 environment is crucial for guiding efficient and sustainable water use.

34 Previous studies on water resource assessment have explored the effects of climate change  
35 and anthropogenic factors on available water resources, including streamflow (Ahiablame et al.,  
36 2017; Tan et al., 2023), baseflow (Ficklin et al., 2016; Tan et al., 2020), lake water (Acero Triana  
37 and Ajami, 2022; Tao et al., 2020), and groundwater (Han et al., 2020). Falkenmark and Rockström  
38 (2006) introduce a novel perspective on water resource assessment by categorizing water resources  
39 into *BW* and *GW*. *BW* is the total of deep aquifer recharge and river streamflow, such as water in  
40 lakes and rivers. Water users such as industries, agriculture, and municipal users can directly utilize  
41 *BW*. On the contrary, *GW* is the portion of precipitation that is not drained to the river for  
42 streamflow generation. *GW* is temporarily retained in the soil before eventually being released

43 back into the air by evapotranspiration. *GW* encompasses both green water flow (*GWF*) and green  
44 water storage (*GWS*) (Veettil and Mishra, 2018; Zang and Liu, 2013). Traditional water resource  
45 assessments concentrate on available water resources and only consider *BW*, but neglect *GW* (Dai  
46 et al., 2022), although *GW* is also essential. *GW* supplies about 80% of total water resources,  
47 sustaining crop growth and the sustainable development of forest and grassland ecosystems in arid  
48 regions or during dry seasons (Li et al., 2018; Schuol et al., 2008). Green water scarcity can lead  
49 to ecosystem degradation and intensify competition between human needs and ecosystems for  
50 water resources (Falkenmark et al., 2003; Veettil and Mishra, 2018). Compared to traditional  
51 streamflow assessment methods, water resource scarcity assessment methods based on the  
52 framework of *BW* and *GW* are more appropriate for maintaining sustainable water resource  
53 management (Cooper et al., 2022; Liu et al., 2017). Recently, some studies have characterized  
54 water scarcity by assessing variations of *BW* and *GW*. For example, Veettil and Mishra (2020)  
55 assess blue water scarcity and green water scarcity to show the water security status of counties in  
56 the United States. Hoekstra et al. (2012) use the concept of *BW* footprint to study water scarcity  
57 issues. Schyns et al. (2019) use the *GW* footprint to investigate green water scarcity and find that  
58 the increasingly severe shortage of *GW* poses a significant threat to natural ecosystems.

59 The impacts of climate change and anthropogenic on the hydrological cycle processes in  
60 watersheds have attracted widespread attention (Ahiablame et al., 2017; Chouchane et al., 2020;  
61 Cooper et al., 2022; Tan et al., 2022b; Veettil and Mishra, 2016). Changes in land use alter the

62 underlying surface conditions. For example, afforestation or deforestation may exacerbate or  
63 alleviate global or regional climate change, and thus affect hydrological cycle processes (Bai et al.,  
64 2020; Lian et al., 2020; Qiu et al., 2023). Changes in land use often lead to alterations in land-  
65 atmosphere interactions, and vegetation cover changes are essential for regulating climate systems  
66 and land ecosystems (Foley et al., 2005; Huang et al., 2020). Large-scale greening could modify  
67 geophysical interactions between the atmosphere and the ground, impacting larger or local regional  
68 hydrological cycles. Land degradation (Walters and Babbar-Sebens, 2016), deforestation (Lee et  
69 al., 2011), and urbanization (Mohan and Kandya, 2015; Zhang et al., 2018) also have far-reaching  
70 effects on the climate and hydrological cycle.

71 Climate change is also crucial to the variations in *BW* and *GW* resources. Precipitation is the  
72 source of *BW* and *GW*, and factors such as temperature, solar radiation, and potential  
73 evapotranspiration significantly influence the changes of *BW* and *GW* in watersheds, especially in  
74 *GWF* (Pandey et al., 2019; Schewe et al., 2014). For a single watershed, *BW* depends directly on  
75 precipitation and evapotranspiration (*GWF*) (Shen et al., 2017; Vano et al., 2012). Furthermore,  
76 precipitation intensity can have a significant impact on the redistribution of precipitation, *BW*, and  
77 *GW*, by altering infiltration and runoff generation processes (Eekhout et al., 2018; Nearing et al.,  
78 2005). Therefore, it is crucial to quantify the effects of climate change and LUCC on *BW* and *GW*  
79 resources in a watershed for effective water resource planning and management.

80 Water resources management is the primary issue to be addressed for water security.

81 Hydrological models are important tools to meet various needs in water resource management.  
82 Hydrological model simulation is an effective method to evaluate changes in blue and green water  
83 resources. As a widely used semi-distributed parametric hydrological model, the SWAT model is  
84 increasingly used in water resources management at the watershed scale. Based on the SWAT  
85 model, researchers simulated the spatiotemporal changes in blue and green water resources in Iran  
86 (Ahiablame et al., 2017), the Yangtze River basin (Nie et al., 2023), the Poyang Lake basin (Liu et  
87 al., 2023), and India (Sharma et al., 2023). Some studies have also used model simulations to  
88 analyze the effects of climate change and human activities on water resource changes in Meki  
89 River basin (Hordofa et al., 2023), China (Liu et al., 2022), and Ningxia(Ahiablame et al., 2017),  
90 etc. However, most of the hydrological models used in the study were calibrated and validated  
91 using only observed streamflow data without checking the accuracy of other simulated water  
92 variables, which can lead to uncertainties in modeling soil moisture and evapotranspiration (Nie  
93 et al., 2023).

94 The Dongjiang River Basin (DRB) is a crucial water source region for core cities in GBA,  
95 such as Shenzhen, Hong Kong, and Huizhou. Given the significant *BW* demand from agriculture,  
96 domestic utilization, and industry, as well as the *GW* demand from over 18,000 km<sup>2</sup> of forested  
97 land, the water resource stress in DRB is extremely high, although DRB is located in the wet South  
98 China (Liu et al., 2018). The growing mismatch between increasing water demand and decreasing  
99 water supply, along with seasonal and pollution-induced water scarcity issues, is becoming

100 increasingly prominent (Yang et al., 2018). However, the majority of current studies on water  
101 resources of DRB focus on changes and scarcity of surface water and groundwater (*BW*) while  
102 overlooking the critical role and spatiotemporal variations of *GW* (Huang et al., 2022; Jiang et al.,  
103 2023; Wu et al., 2021). With the high-intensity urbanization and climate change in DRB, changes  
104 of *BW* and *GW* resources in DRB remain unknown.

105 This research aims to analyze the influence of climate change and LUCC on *BW* and *GW* in  
106 DRB. The objectives of this research are (a) to build the SWAT model for DRB hydrological  
107 simulation, (b) to quantitatively evaluate the spatial and temporal variation of *BW* and *GW* in DRB,  
108 (c) to assess the status of water scarcity in DRB using the framework of *BW* and *GW* resources,  
109 and (d) to estimate the effects of climate change and LUCC on *BW* and *GW* in DRB.

## 110 **2 Materials and methods**

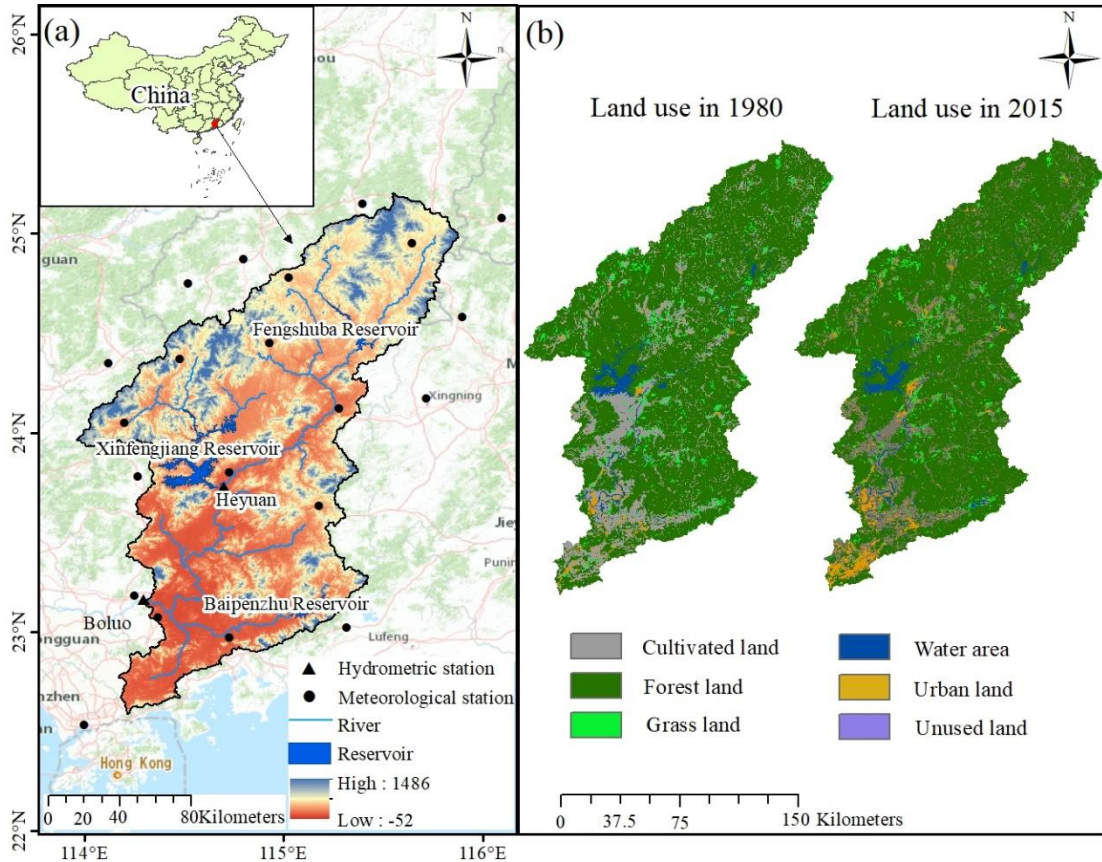
### 111 2.1 Study area

112 The Dongjiang River is an important tributary of the Pearl River, positioned between  
113 longitude 113°25'-115°52'E and latitude 22°26'-25°12'N. It originates in Xunwu County, Jiangxi  
114 Province, flows through Jiangxi and Guangdong provinces, and goes across major cities including  
115 Longchuan, Heyuan, Dongguan, and Shenzhen. The trunk stream of the Dongjiang River has a  
116 total length of 562 km. DRB covers a watershed area of  $3.5 \times 10^4$  km<sup>2</sup>. DRB is of in the subtropical  
117 monsoon climate zone with adequate precipitation and high temperatures. The average annual

118 precipitation ranges from 1500-2400 mm, and the average temperature of the basin is 21°C (Wu  
119 et al., 2019a). The altitude of the basin decreases from the northeast to the southwest. Regions of  
120 the upper reaches of DRB are dominated by mountains and hills, those of the middle reaches of  
121 DRB are dominated by hills and plains, and those of the lower reaches of DRB are dominated by  
122 plains.

123 Previous hydrological simulation studies of DRB mainly use the Boluo hydrometric station  
124 as the outlet of the watershed (He et al., 2013; Wu et al., 2019a), so this research only analyzes the  
125 area of DRB where water flows to the Boluo station (Fig. 1). The Boluo hydrometric station is the  
126 main control station in the lower reaches of the Dongjiang. The Boluo hydrometric station occupies  
127 a drainage area of 25,325 km<sup>2</sup>, which is 71.7% of the total area of DRB. Since the 1950s, more  
128 than 896 reservoirs, ponds, dams, and other water conservancy facilities have been constructed in  
129 DRB. Among them, the Baipenzhu Reservoir, Fengshuiba Reservoir, and Xinfengjiang Reservoir  
130 are the three largest reservoirs in the basin with a cumulative storage capacity of 17,048 million  
131 m<sup>3</sup>. The Dongjiang-Shenzhen Water Supply Project constructed in 1964 diverts water from the  
132 Dongjiang River to Shenzhen and Hong Kong for providing fresh water resources for municipal  
133 use. Over 70% of Hong Kong's freshwater supply comes from the Dongjiang River. Therefore, it  
134 is crucial to comprehend the shifts in water resources within DRB for projecting future available  
135 water resources for the development of GBA.





136  
 137 Figure 1. Location and characteristics of the study area: (a) location of the watershed, spatial distribution of the  
 138 hydrometeorological stations, and digital elevation model (Farr et al., 2007), (b) land use map (Xu et al.,  
 139 2018).

## 140 2.2 Methodology

### 141 2.2.1 SWAT model

142 The SWAT model was adopted to simulate hydrological processes and estimate the amount  
 143 of *BW* and *GW* for DRB (Arnold et al., 1998; Neitsch et al., 2002). The SWAT model is widely  
 144 applied to simulate streamflow and surface runoff (Arshad et al., 2022; Martínez-Salvador and  
 145 Conesa-García, 2020; Nie et al., 2023). The SWAT model is also widely utilized for exploring  
 146 changes in *BW* and *GW* (Dai et al., 2022; Liang et al., 2018; Schuol et al., 2008).

147 In SWAT modeling, DRB was divided into 63 sub-basins (Fig. S1), and each sub-basin was  
148 then categorized into Hydrologic Response Units (HRUs) depending on land use, soils, and slope.  
149 The SCS curve number method was used for flow partitioning according to land use, soil type and  
150 antecedent soil moisture. The Penman-Monteith method was used to calculate potential  
151 evapotranspiration, which comprehensively considered various climatic factors such as solar  
152 radiation, air temperature, wind speed and relative humidity (Arnold et al., 1998; Neitsch et al.,  
153 2002).

#### 154 2.2.2 Model calibration and validation

155 ~~In order to~~To reduce the influence of hydraulic engineering, the SWAT model was calibrated  
156 and validated by utilizing monthly restored natural streamflow at the Boluo and Heyuan  
157 hydrometric stations. The optimum model parameters are shown in Table 1. All the selected  
158 parameters are automatically calibrated with 500 simulations via SWAT-CUP. The warm-up period  
159 for model simulations is the first two years of the simulation period. Reconstructed natural  
160 streamflow in 1970-1979 was used to calibrate the model, and monthly time series of reconstructed  
161 natural streamflow, *ET* from GLEAM, and soil moisture data from ERA5 during 1980-1989 were  
162 used to validate the model. The calibration period for this research was 1970-1979, and the  
163 validation period was 1980-1989. Three metrics, including the determination coefficient ( $R^2$ ), the  
164 percentage bias (*PBIAS*), and Nash-Sutcliffe efficiency (*NSE*) were applied to evaluate the  
165 simulation performance of the SWAT model:

166 
$$NSE = 1 - \frac{\sum_{i=1}^n (Q_{nat} - Q_{sim})^2}{\sum_{i=1}^n (Q_{nat} - Q_{ave})^2} \quad (1)$$

167 
$$PBIAS = \frac{\overline{Q_{sim}} - Q_{ave}}{Q_{ave}} \times 100 \quad (2)$$

168 
$$R^2 = \left[ \frac{\sum_{i=1}^n (Q_{nat} - Q_{ave})(Q_{sim} - \overline{Q_{sim}})}{\sqrt{\sum_{i=1}^n (Q_{nat} - Q_{ave})^2 \sum_{i=1}^n (Q_{sim} - \overline{Q_{sim}})^2}} \right]^2 \quad (3)$$

169

170 where  $Q_{nat}$ ,  $Q_{ave}$ ,  $Q_{sim}$ , and  $\overline{Q_{sim}}$  are monthly natural streamflow, mean monthly natural  
 171 streamflow, simulated streamflow, and mean monthly simulated streamflow, respectively.  $n$  is the  
 172 total number of time step.

173 Table 1 Range of the main parameters and their optimal values obtained from the model calibration

Parameter	Calibration type	Initial range	Best calibrated value
GW_REVAP.gw	V	0.19-0.2	0.199
GWQMN.gw	V	493-1247	916.493
SLSUBBSN.hru	R	2.6-5.7	2.804
ESCO.hru	V	0.89-0.97	0.901
CN2.mgt	R	0.14-0.27	0.209
CH_K2.rte	V	0.38-1.16	0.926
ALPHA_BNK.rte	V	0.12-0.18	0.165
SOL_AWC.sol	R	0.3-0.6	0.598
SOL_K.sol	R	0.32-0.69	0.669
CH_K1.sub	V	0-0.15	0.0295

Note: The symbols of V and R denote a replacement and a relative change to the default parameter value, respectively.

174 This study reconstructed the natural monthly streamflow series of the basin by combining the  
 175 inflow and outflow of the three major reservoirs (Xinfengjiang Reservoir, Fengshuba Reservoir,  
 176 and Baipenzhu Reservoir) in DRB, based on the watershed water balance (Tu et al., 2018):

177 
$$Q_{nat} = Q_o + \Delta Q = Q_o + Q_{in} - Q_{out} \quad (4)$$

178 where  $\Delta Q$  is the total reduced water volume,  $Q_o$ ,  $Q_{in}$ , and  $Q_{out}$  are the observed streamflow,  
179 reservoir inflow, and reservoir outflow, respectively.

## 180 2.3 Calculation of blue and green water and water security indicators

### 181 2.3.1 Calculation of blue and green water

182  $BW$  is calculated from the sum of water yield (SWAT output WYLD) and groundwater storage.  
183 The former refers to the amount of water that leaves the HRU and enters the channel. The latter  
184 represents the net amount of water recharged to aquifers (SWAT output GW\_RCHG) and the  
185 amount of aquifer water discharges to the main channel (SWAT output GW\_W) during a time step  
186 (Hordofa et al., 2023).  $GW$  can be divided into two components including  $GW_F$  which is the actual  
187 evapotranspiration (SWAT output ET) from the HRU, and  $GW_S$  which is the soil water moisture  
188 (SWAT output SW) (Nie et al., 2023; Veettil and Mishra, 2018). The calculation of the Green Water  
189 Index ( $GWI$ ) involves dividing the quantity of  $GW$  by the sum of  $BW$  and  $GW$  (Ding et al., 2024).

### 190 2.3.2 Blue and green water scarcity

191 Blue water scarcity ( $BWSC$ ) is determined by the quotient of  $BW$  withdrawal and availability.  
192 The estimation of  $BW$  withdrawals ( $BWW$ ) in this study involved the multiplication of the  
193 aggregate population in each sub-basin by the combined water consumption per person (Liang et

194 al., 2020). The population of each sub-basin was extracted from the population raster data. Blue  
 195 water availability (*BWA*) represents the quantity of water that can be utilized without negatively  
 196 impacting the river ecosystems. Exhaustive exploitation of *BW* in rivers may adversely impact  
 197 river ecosystems. Previous studies have generally used environmental flow requirements (*EFR*) as  
 198 a suitable metric for sustaining robust ecosystems (Honrado et al., 2013). According to the study  
 199 of Richter (2010) and Richter et al. (2012), extracting more than 20% of the water from rivers may  
 200 result in ecological degradation. Therefore, 20% of streamflow can be deemed *BW* and used for  
 201 water supply (Veettil and Mishra, 2016). The calculation of *EFR*, *BWA*, and *BWSC* are as follows:

$$202 \quad EFR_{(a,t)} = 0.8 \times Q_{\text{mean}(a,t)} \quad (6)$$

203 where  $EFR_{(a,t)}$  is the *EFR* for sub-basin ‘*a*’ during time ‘*t*’;  $Q_{\text{mean}}$  is the long-term monthly average  
 204 streamflow.

$$205 \quad BWA_{(a,t)} = Q_{(a,t)} - EFQ_{(a,t)} \quad (7)$$

$$206 \quad BWSC = BWW / BWA \quad (8)$$

207 Green water scarcity (*GWSC*) is defined as the ratio between green water footprint (*GWFO*)  
 208 and green water availability (*GWA*). *GWFO* denotes the actual evapotranspiration from the  
 209 watershed. *GWA* is the soil moisture that is available for evapotranspiration and vegetation  
 210 transpiration and is equal to the initial soil moisture (Liang et al., 2020). The *GWSC* can be  
 211 formulated as:

$$212 \quad GWSC_{(a,t)} = GWFO_{(a,t)} / GWA_{(a,t)} \quad (9)$$

213 where  $GWSC$  is green water scarcity;  $GWFO_{(x,t)}$  is the actual evapotranspiration;  $GWA_{(a,t)}$  is initial  
214 soil moisture.

215 Based on the blue water scarcity and green water scarcity, water scarcity of a region is  
216 categorized as: mild scarcity, moderate scarcity, severe scarcity and extreme scarcity, with  
217 thresholds set at 100%, 150% and 200%, respectively.

### 218 2.3.3 Regional water stress

219 The Falkenmark index ( $FLK$ ) (Falkenmark et al., 1989) is a widely used measure of water  
220 stress, defined as the proportion of  $BWA$  to the overall population. The Falkenmark index is  
221 classified into no stress, stress, scarcity, and absolute scarcity based on per capita water use.  
222 Absolute scarcity is regarded to occur in areas where the indicator threshold is less than  $500 \text{ m}^3$   
223  $\text{capita}^{-1} \text{ a}^{-1}$ , and no stress is thought to occur in areas where the threshold is larger than  $1700 \text{ m}^3$   
224  $\text{capita}^{-1} \text{ a}^{-1}$ .

## 225 2.4 Calculation of relative contribution

### 226 2.4.1 Scenario design and simulation

227 Three scenarios were constructed to assess the impacts of climate change and LUCC on  $BW$   
228 and  $GW$  by changing climate conditions (land use) while holding land use (climate conditions) for  
229 the three scenarios simulation each (Table 2). The land use map was fixed when simulating the  
230 influences of climate change on blue and green water (S2-S1), while climate conditions was fixed

231 when simulating the influences of LUCC on blue and green water (S3-S2). The climate conditions  
 232 and the land use were altered when assessing the joint influences of climate change and LUCC on  
 233 blue and green water (S3-S1).

234 Table 2 Scenario settings for the simulation of effects of climate change and LUCC on blue and green water

Scenarios	Land use	Climate period	Combined effects	Land use change effects	Climate change effects
S1	1980	1970-1993			
S2	1980	1994-2017			S2-S1
S3	2015	1994-2017	S3-S1	S3-S2	

235 2.4.2 Relative contribution rate calculation

236 The influences of climate change and LUCC on the changes of blue and green water in  
 237 different periods are evaluated utilizing the relative contribution (*RC*) in this research (Li et al.,  
 238 2021):

239 Climate change contribution to *BW* and *GW* change is estimated by:

240 
$$RC_C = \frac{|X_2 - X_1|}{|X_2 - X_1| + |X_3 - X_2|} \times 100\% \quad (10)$$

241 where  $X_1$ ,  $X_2$ , and  $X_3$  are the amount of water including *BW* or *GW* and *GWS*, respectively for  
 242 scenarios S1, S2, and S3.

243 The contribution of LUCC to changes in *BW* and *GW* are estimated by Equations 11.

244 
$$RC_L = \frac{|X_3 - X_2|}{|X_3 - X_2| + |X_2 - X_1|} \times 100\% \quad (11)$$

## 245 2.5 Data

246 The dataset used in this study consists of three parts: (1) hydrometeorological data, (2)  
247 geospatial data encompassing DEM, soil type, and land use, and (3) socioeconomic data  
248 encompassing per capita water consumption and population data.

249 Observed monthly streamflow data of the two hydrological stations in the study were  
250 collected for the years 1970-2000 from Boluo Station and Heyuan Station, and the observed  
251 streamflow time series of these two hydrological stations are of no missing data. Monthly inflow  
252 and outflow data of the three major reservoirs in DRB were also collected. All hydrologic data  
253 were obtained from the Guangdong Provincial Hydrological Bureau. Meteorological data of daily  
254 precipitation, temperature, and other meteorological data for 1968-2017 from 21 Meteorological  
255 stations in the watershed were obtained from the National Meteorological Information Center of  
256 the China Meteorological Administration. Monthly actual *ET* data for SWAT model validation was  
257 obtained from the Amsterdam Evapotranspiration Model dataset with a spatial resolution of  $0.25^\circ$   
258  $\times 0.25^\circ$  (Martens et al., 2017). Monthly soil moisture data for SWAT model validation was obtained  
259 from the European Center for Medium-Range Weather Forecasts ERA5-land dataset with a spatial  
260 resolution of  $0.1^\circ \times 0.1^\circ$  (Muñoz Sabater, 2019). The actual evapotranspiration and soil moisture  
261 of the watershed equals the average of all grids included in DRB.

262 The 90-meter resolution DEM data and 30-meter resolution land use data at ten-year intervals  
263 (i.e., 1980, 1990, 2000, 2010, 2015) are obtained from the Data Center for Resources and



264 Environmental Sciences of the Chinese Academy of Sciences (Xu et al., 2018). Soil data is  
265 obtained from the 1-km resolution Harmonized World Soil Database dataset from the Food and  
266 Agriculture Organization of the United Nations (Fischer et al., 2008).

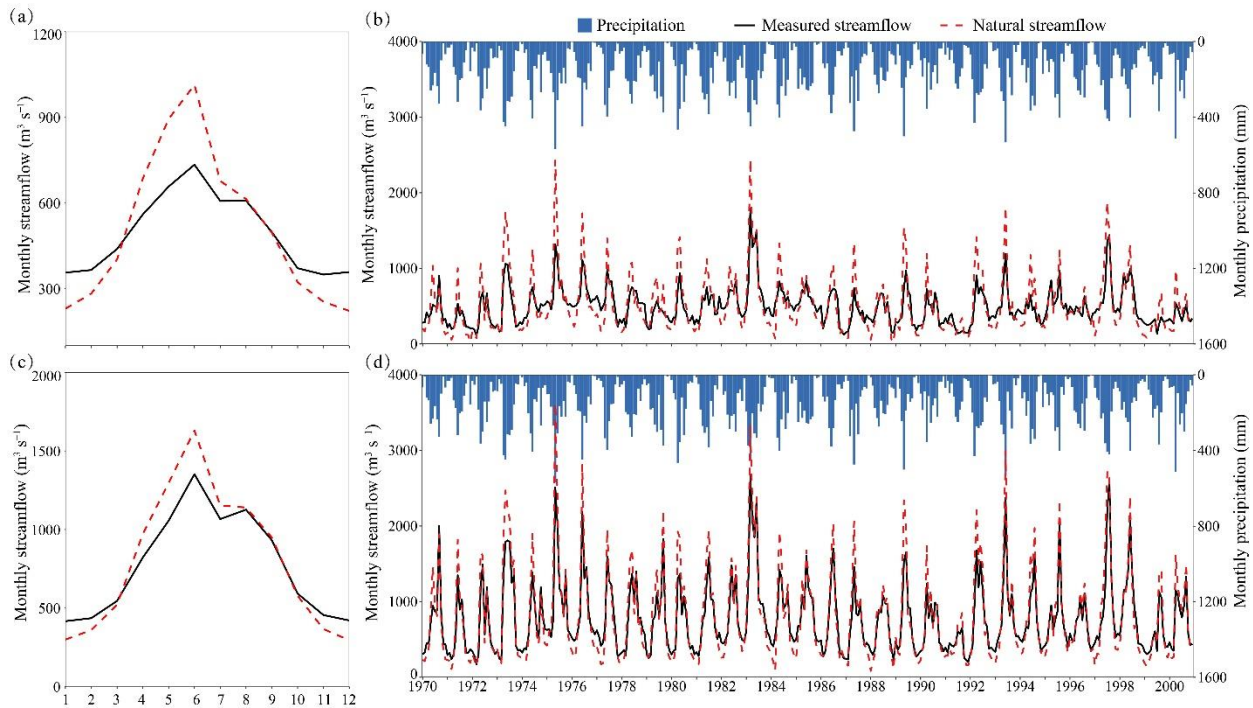
267 The annual per capita integrated water consumption data of DRB from 2000-2017 was  
268 acquired from the Water Resources Bulletin of Guangdong Province. The population data in 2000,  
269 2005, 2010, and 2015 was obtained from the  $1 \times 1$  km spatial raster data of the Resource and  
270 Environment Science and Data Center of the Chinese Academy of Sciences (Xu, 2017).

## 271 **3 Results**

### 272 3.1 Model Performance

#### 273 3.1.1 Streamflow reconstructed

274 The difference between the monthly average observed streamflow and the monthly average  
275 natural streamflow is small (Figure 2). The monthly average measured streamflow and natural  
276 streamflow at the Heyuan station is  $492.1 \text{ m}^3 \text{ s}^{-1}$  and  $507.9 \text{ m}^3 \text{ s}^{-1}$ , respectively, while the monthly  
277 average measured streamflow and natural streamflow at the Boluo station is  $768.4 \text{ m}^3 \text{ s}^{-1}$  and  $796.7$   
278  $\text{m}^3 \text{ s}^{-1}$ , respectively. The difference between the measured streamflow and the natural streamflow  
279 mainly occurs in November, December, January, and February (where the measured streamflow is  
280 greater than the natural streamflow) and May, June, and July (where the measured streamflow is  
281 less than the natural streamflow) (Fig. 2a and Fig. 2c).

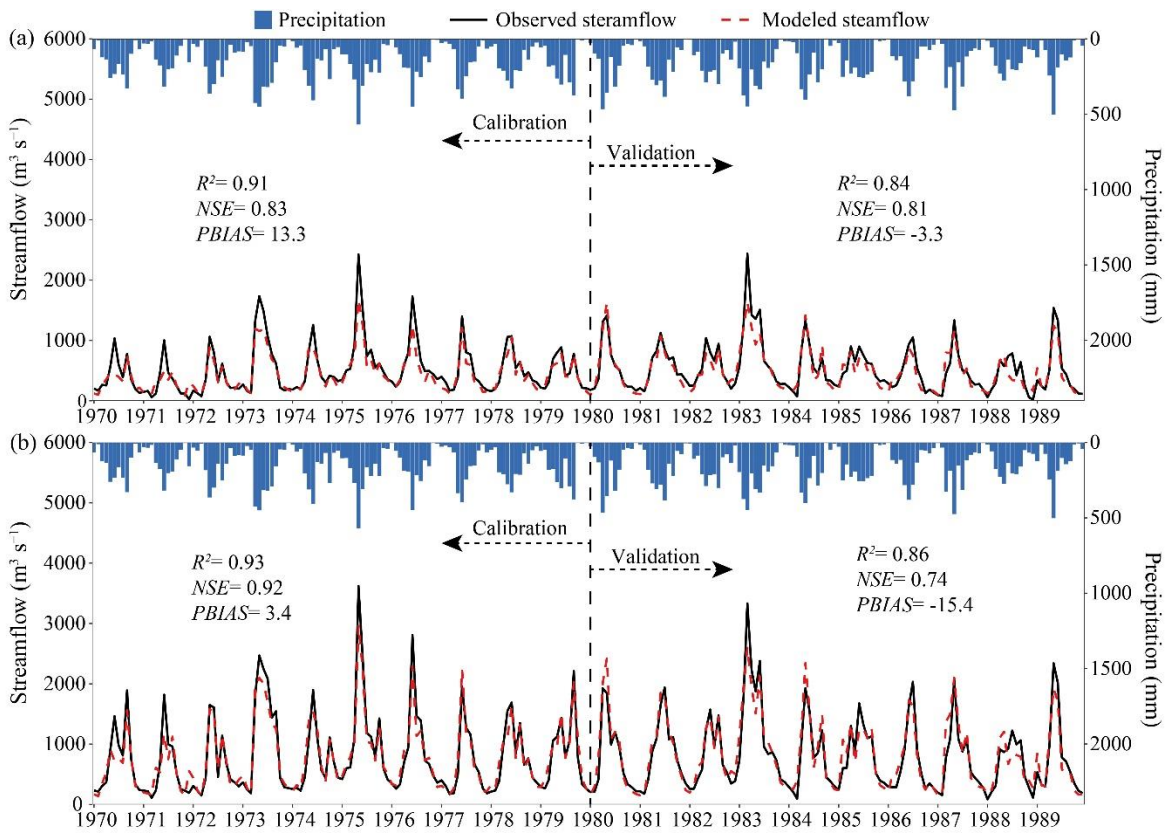


282  
 283 Figure 2. Observed streamflow and natural streamflow processes at the Heyuan and Boluo stations from 1970  
 284 to 2000. (a) Annual distribution of streamflow at the Heyuan station, (b) streamflow process at the Heyuan station,  
 285 (c) annual distribution of streamflow at the Boluo station, (d) streamflow process at the Boluo station

286 3.1.2 Model calibration and verification

287 The SWAT model shows sufficient accuracies in simulating streamflow, actual  
 288 evapotranspiration, and soil moisture changes in DRB and can better simulate both seasonal and  
 289 interannual changes in streamflow. During the calibration period, both stations achieved  $R^2$  above  
 290 0.9,  $NSE$  exceeding 0.8, and  $PBIAS$  less than 14% (Fig. 23). Both stations had simulated  
 291 streamflow  $R^2$  greater than 0.8 during the validation period. The  $NSE$  for streamflow simulation at  
 292 the Heyuan station and Boluo station of the validation were 0.81 and 0.74, respectively. The model  
 293 performs well in simulating the  $ET$  and soil moisture. Since the GLEAM  $ET$  data and ERA5 soil  
 294 moisture data are raster data of spatial resolution of  $0.25 \times 0.25^\circ$ , considering the influence of data

295 accuracy on the results, this study uses the watershed scale to validate the simulation results of *ET*  
 296 and soil moisture. In the validation period, the  $R^2$  and *NSE* for the simulation of evapotranspiration  
 297 were 0.92 and 0.8, respectively (Fig. S2), while the  $R^2$  and the *NSE* for the soil moisture simulation  
 298 were both greater than 0.6. These validation results show that the model can be used to simulate  
 299 hydrological regimes in DRB.



300  
 301 Figure 23. Simulated and observed monthly streamflow at the (a) Heyuan and (b) Boluo gauge stations  
 302 during calibration and validation periods.

303

### 304 3.2 LUCC and Climate variability in DRB

305 LUCC in DRB is mainly the decrease of cultivated land and the increase of urban land. The

306 land use in DRB primarily consisted of forest land (18,875-18833 km<sup>2</sup>), which is more than 70%  
 307 of DRB. From 1980 to 2015, the urban land and water areas showed an increase of 469.4 km<sup>2</sup>  
 308 (137%) and 17.4 km<sup>2</sup> (2.8%), while the grassland, cultivated land, and forest land showed a  
 309 decrease of 41.3 (4.3%), 487.5 (10.8%), and 42.1 km<sup>2</sup> (0.2%), respectively (Table 3).

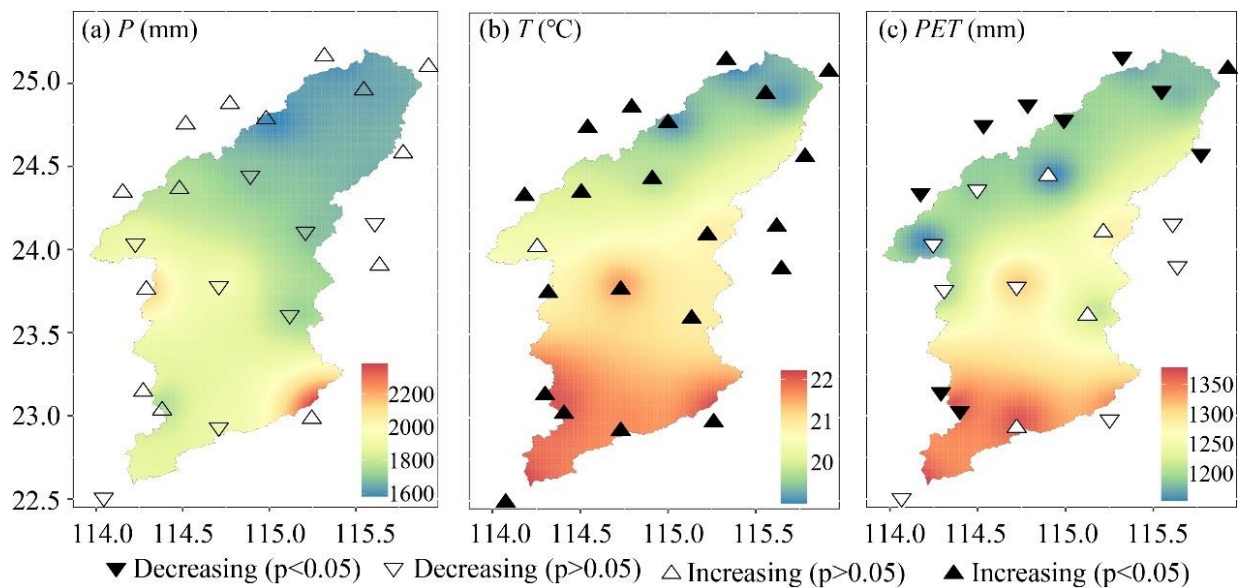
310 Table 3 Land use transfer matrix in DRB from 1980 to 2015

Land use type	2015						1980 total (km <sup>2</sup> )
	Grass Land (km <sup>2</sup> )	Urban land (km <sup>2</sup> )	Cultivated Land (km <sup>2</sup> )	Forest land (km <sup>2</sup> )	Water area (km <sup>2</sup> )	Unused land (km <sup>2</sup> )	
1980 Grassland	795.6	29.9	18.3	123.5	2.5	0.0	969.7
Urban land	0.6	319.6	12.4	7.6	2.3	0.0	342.4
Cultivated land	19.0	269.8	3771.7	427.9	40.4	0.03	4528.8
Forest land	110.7	183.7	226.2	18278.7	33.1	0.02	18832.5
Water area	2.5	8.9	12.7	36.8	551.0	0.00	611.9
Unused land	0.0	0.0	0.02	0.03	0.00	0.45	0.51
2015 total	928.4	811.9	4041.3	18874.5	629.2	0.51	25285.8

311 DRB exhibited significant regional differences in multi-year average precipitation,  
 312 temperature, and potential evapotranspiration. The precipitation exhibited an increasing trend from  
 313 the central to the south and north of DRB. The temperature and potential evapotranspiration  
 314 showed an overall distribution pattern of greater values in the south and minor values in the north  
 315 of DRB (Fig. 34). The multi-year average precipitation for the entire DRB was 1790.1 mm, with  
 316 annual precipitation ranging from 1236.2-2567.5 mm. The regions with the highest multi-year  
 317 average annual precipitation are located in the southeast of DRB, where annual precipitation  
 318 exceeds 2200 mm, while the regions with the lowest precipitation are in the northeastern of the

319 watershed. The average annual temperature in DRB ranged from 19.5-21.3 °C, and the average  
 320 annual potential evapotranspiration ranged from 1101.5-1320.6 mm. The south of DRB is  
 321 predominantly urban, characterized by the urban heat island effect, while the north of DRB is  
 322 mountainous with higher elevations, leading to the spatial distribution of temperatures.

323 The average temperature and potential evapotranspiration at DRB meteorological stations  
 324 exhibited significant variations, while precipitation showed a relatively minor trend (Fig. 34).  
 325 Overall, basin-averaged precipitation and potential evapotranspiration showed a non-significant  
 326 decreasing trend, while temperatures showed a significant increasing trend. There was no  
 327 significant change trend of precipitation for all stations in DRB (Fig. 3a4a). Twenty out of 21  
 328 meteorological stations in the region showed statistically significant increasing trends in average  
 329 temperature, indicating a warming trend (Fig. 3b4b). Nine stations showed a significant decreasing  
 330 trend in potential evapotranspiration, primarily located in northern DRB (Fig. 3c4c).



331  
 332 Figure 34. Spatial distribution of annual mean (a) precipitation, (b) temperature, (c) potential

333 evapotranspiration in DRB from 1960-2017. Each triangle represents the Mann-Kendall test result at a  
334 meteorological station.

335 The mean precipitation, temperature, and potential evapotranspiration of DRB can be  
336 obtained from the precipitation, temperature, and potential evapotranspiration of stations using the  
337 Tyson polygon method. The inter-annual variation of annual precipitation in DRB showed an  
338 insignificant decreasing trend ( $-0.51\text{mm a}^{-1}$ ). The annual mean temperature showed a significant  
339 increasing trend ( $0.024^{\circ}\text{C a}^{-1}$ ). The annual potential evapotranspiration showed a significant  
340 decreasing trend ( $-0.38\text{mm a}^{-1}$ ) (Fig. S3).

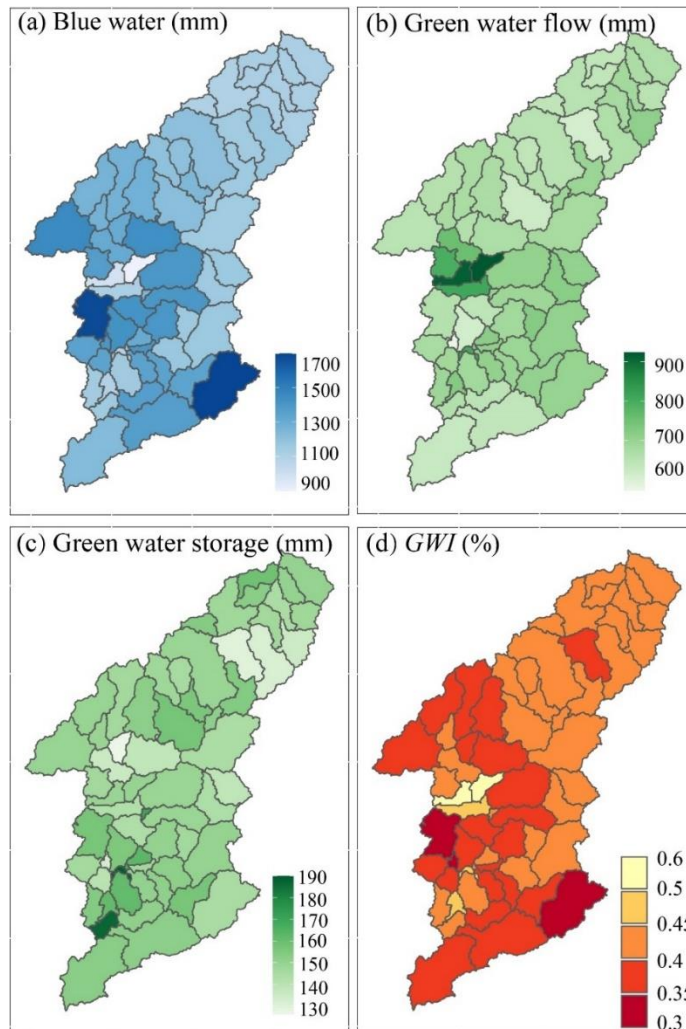
### 341 3.3 Blue and green water resources

342 The average annual *BW* and *GW* were 1240.8 and 840.7 mm, respectively. The DRB water  
343 resources were dominated by *BW*, representing 60.1% of the total water resources, and *BW* was  
344 1.48 times higher than that of *GW* resources. The average *GWF* and *GWS* were 689.3 and 151.4  
345 mm, respectively.

346 The annual *BW* resources in the sub-basins of DRB ranged from 893.7-1990 mm, showing  
347 an increasing trend from the central to the south and north of DRB, aligning with the spatial  
348 distribution of precipitation (Fig. 4a5a). The regions with abundant *BW* resources are situated in  
349 the central and southeast parts of DRB ( $>1300$  mm), and the *BW* in the upper reaches is  
350 comparatively low ( $<1100$  mm). Differences in the spatial distribution of *BW* are primarily caused  
351 by differences in the spatial distribution of precipitation. Overall, the *GWF* and *GWS* are more  
352 evenly distributed in the sub-basins than *BW*. The annual *GWF* in the sub-basins of DRB ranged

353 from 573.6-923.6 mm. The sub-basins with higher *GWF* are primarily located in the Xinfengjiang  
354 reservoir area in the middle reaches (>700 mm), while the low *GWF* sub-basins are situated in the  
355 southwest of DRB (<600 mm) (Fig. 4b5b). The land use in the sub-basins where Xinfengjiang  
356 Reservoir is located is primarily water areas, with a higher water evaporation rate than other  
357 regions, resulting in a greater *GWF* in this area than in other regions. The annual *GWS* in the sub-  
358 basins of DRB ranged from 126-190.6 mm. The sub-basins with higher *GWS* are mainly located  
359 in the lower part of DRB (>150 mm) (Fig. 4e5c). The distribution pattern of *GWS* resources has a  
360 great relationship with the soil type of the watershed. The upper reaches and the northwestern part  
361 of the watershed are mostly red soil, while the middle and lower reaches are dominated by reddish  
362 soil. Reddish soil has a smaller water storage capacity than red soil, loses water faster, and has  
363 weaker water conservation and water supply performance than red soil. This is the primary factor  
364 for the north-south discrepancies in the amount of *GWS* resources in DRB. In addition, the southern  
365 region is mostly of large and medium-sized cities. As urban construction land expands, the land  
366 use type in the region has gradually changed to urban land, industrial land, etc., and the  
367 solidification of road surfaces has reduced the area of bare soil in the region, resulting in a decrease  
368 in *GWS* resources. The annual *GWI* (Fig. 4d5d) showed a spatial pattern opposite to *BW*,  
369 decreasing from 0.45 in the upper reaches to 0.3 in the lower reaches. The highest *GWI* is found  
370 in the upper reaches, which is due to the relatively low rainfall in the upper reaches and the lush  
371 vegetation, with significant plant interception and transpiration, resulting in a higher proportion of

372 total evapotranspiration than in the middle and lower reaches. The central part of the basin has the  
 373 highest precipitation, leading to a lower *GWI*. The southern part of the watershed has the highest  
 374 temperature, and evapotranspiration is high. Meanwhile, the lower reaches have a large proportion  
 375 of agricultural and urban land, and crop irrigation can increase evapotranspiration.

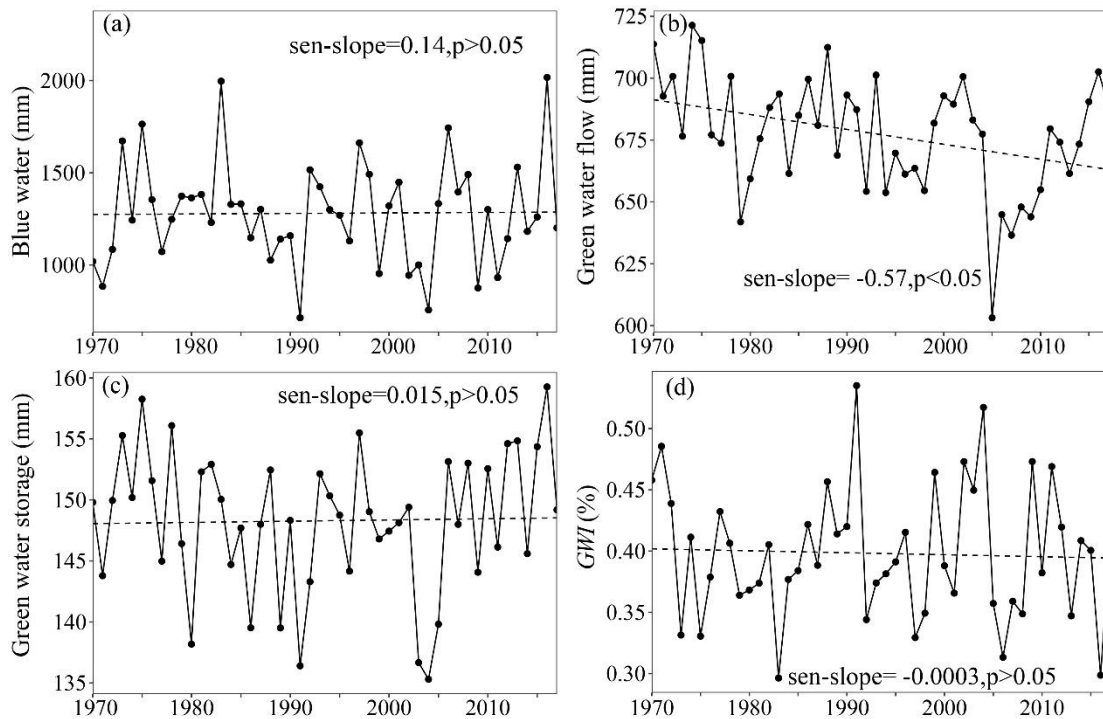


376  
 377 Figure 45. Spatial distribution of mean (a) *BW*, (b) *GWF*, (c) *GWS*, (d) *GWI* in DRB over ~~during~~ 1970-  
 378 2017.

379 In DRB, there was no significant increasing trend in either *BW* or *GWS*, while *GWF*  
 380 exhibited a significant decreasing trend. The annual trend rate of *BW* in DRB was 0.14 mm a<sup>-1</sup>,



381 with an annual fluctuation range of 713.6-2017.5 mm during 1970-2017. The minimum BW  
 382 occurred in 1991, while the maximum was recorded in 2016 (Fig. 5a4a). The GWF in DRB from  
 383 1970 to 2017 exhibited a significant decreasing trend (-0.57 mm a-1) (Fig. 5b4b). The minimum  
 384 GWF occurred in 2005 (603.1 mm), while the maximum was recorded in 1974 (721.3 mm). In  
 385 contrast, the GWS in DRB from 1970 to 2017 has been slowly increasing at a rate of 0.015 mm a-  
 386 1 (Fig. 5c4c). The annual fluctuation in GWS was smaller than BW and GWF. The GWI in DRB  
 387 from 1970 to 2017 showed no significant decreasing trend at a rate of -0.0003 % a-1 ( $p>0.05$ ) (Fig.  
 388 5d4d), implying that the redistribution of precipitation in DRB might change slowly.



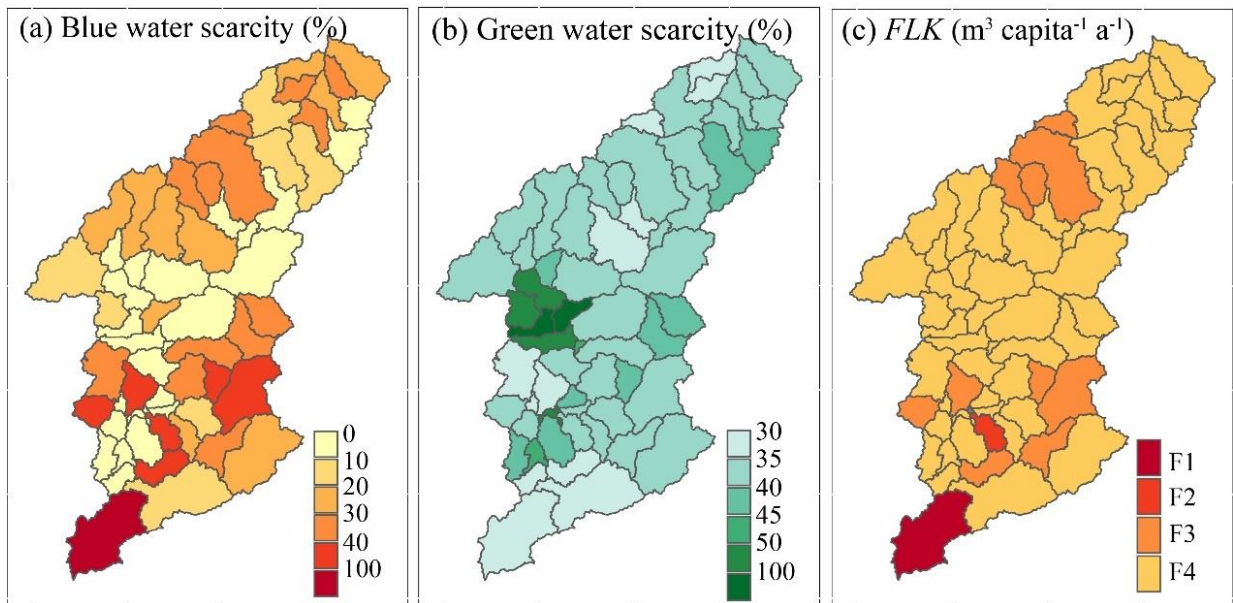
389  
 390 Figure 56. Interannual variation of (a) *BW*, (b) *GWF*, (c) *GWS*, (d) *GWI* in DRB during 1970-2017.

### 391 3.4 Blue and green water scarcity

392 The average blue water scarcity level in DRB was low (22.4%) during 1970-2017. The blue

393 water scarcity levels in various sub-basins ranged from 0.1-206%. The multi-year average blue  
394 water scarcity, except for one sub-basin in the southwest, was all low (<100%) (Fig. 6a7a). This  
395 indicates that blue water scarcity is not common in DRB at the annual scale. Regions with  
396 relatively high blue water scarcity (>20%) are mostly situated in the upper reaches of various  
397 tributaries within the watershed, where river streamflow is relatively small. The area with the  
398 highest blue water scarcity (206%) is located in the 63rd sub-basin of Shenzhen and Huizhou,  
399 reaching a moderate level of blue water scarcity. This region has a large population, with a much  
400 higher blue water demand than other areas. Additionally, this sub-basin is situated in the upper  
401 reaches of the primary tributary of DRB, resulting in a limited supply of *BW* resources. Although  
402 the northern parts of sub-basins 55, 56, and 61 have large populations, these sub-basins are situated  
403 in downstream of the main Dongjiang River, with a higher streamflow, leading to lower *BWSC*  
404 levels. The average *GWSC* in the entire basin from 1970-2017 was low (41.4%). The blue water  
405 scarcity levels in various sub-basins ranged from 31-104%. The vegetation cover in DRB is high,  
406 and DRB is thus of relatively high rates of vegetation transpiration and interception evaporation.  
407 The basin experiences a *GWSC* of nearly 50%, indicating a potential occurrence of *GWSC*. The  
408 areas with higher *GWSC* are primarily situated in the middle reaches for DRB (Fig. 6b7b), where  
409 water surface evaporation is high, resulting in their *GWSC* exceeding 100%. The evaporated water  
410 in these areas originates from the reservoirs, not the soil, leading to an overestimation of the *GWSC*  
411 in these sub-basins.

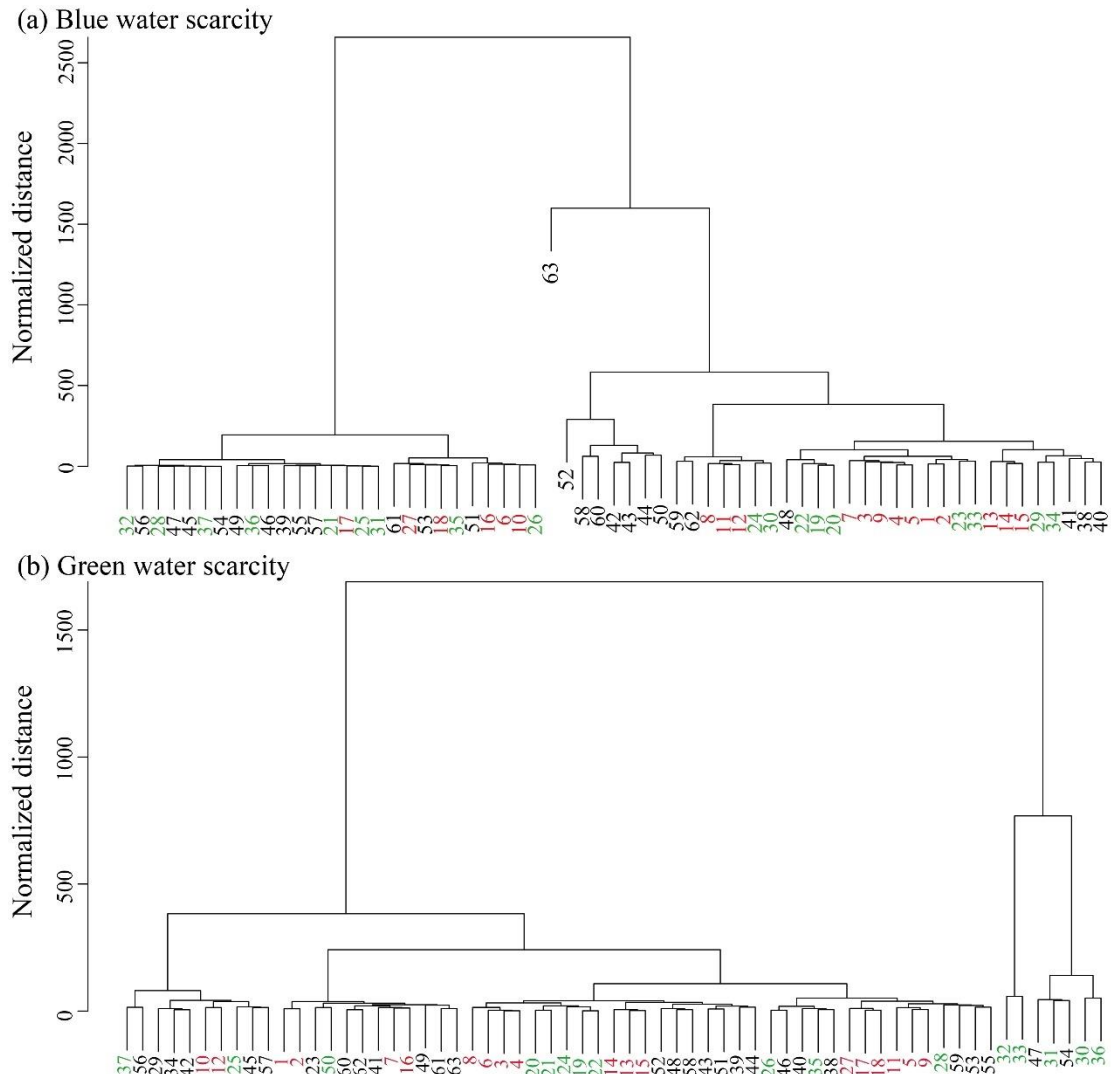
412 Furthermore, the *FLK* index was also used to quantify population-driven water resource  
 413 scarcity. F1-F4 represent absolute scarcity, scarcity, stress, and no stress, respectively. The results  
 414 showed that most regions in DRB have no water scarcity pressure (Fig. 6e7c). However, the 63rd  
 415 sub-basin experienced absolute water scarcity, and the 52nd sub-basin experienced water scarcity.  
 416 There were six lower reaches sub-basins and four upper reaches sub-basins facing water stress.  
 417 DRB receives ample precipitation, resulting in a relatively large river flow, generally leading to a  
 418 higher *FLK* index. As a result, the basin faces lower water resource pressure.



419  
 420 Figure 67. Spatial distribution of the mean (a) *BWSC*, (b) *GWSC*, and (c) *FLK* index in DRB over during  
 421 1970-2017.

422 This study also further identified hotspots of *BWSC* and *GWSC* in DRB by hierarchical  
 423 clustering of *BWSC* and *GWSC* in each sub-basin. Figure 7-8 shows the clustering tree results for  
 424 *BWSC* and *GWSC*. When the standardized distance was set to 500, all sub-basins could be divided  
 425 into four categories according to blue water scarcity: (1) The first category consisted of 27 sub-

426 basins, such as 32, 56, and 28, where the blue water scarcity level was the lowest (<20%). (2) The  
427 second category comprised sub-basin 63, which has the most severe blue water scarcity (206%).  
428 (3) The third category comprised seven sub-basins, such as 52, 58, and 60, all located in the lower  
429 reaches, with relatively high blue water scarcity levels (40%-100%). These sub-basins are mostly  
430 located in the tributaries of the lower reaches, with a relatively large population and smaller river  
431 streamflow compared to the mainstem of the Dongjiang River. (4) The fourth category consisted  
432 of 28 sub-basins, such as 59, 62, and 8, with blue water scarcity levels ranging from 20% to 40%.  
433 Similarly, hierarchical clustering was conducted for *GWSC*. When the standardized distance was  
434 set to 500, *GWSC* in the sub-basins could be divided into three categories: (1) The first category  
435 consisted of 56 sub-basins, such as 37, 56, and 29, with relatively low *GWSC* levels, all below  
436 50%, indicating low *GWSC*. (2) The second category consisted of sub-basins 32 and 33, where the  
437 predominant land use type was water areas, leading to higher *GWSC* due to high water surface  
438 evaporation. (3) The third category consisted of sub-basins 47, 31, 54, 30, and 36, where the water  
439 area proportion in these sub-basins was larger than in others, leading to significant influences from  
440 water surface evaporation. Figure S4 shows the annual variation of blue water scarcity and green  
441 water scarcity in the basin. Except for some sub-basins, the blue and green water scarcity in most  
442 sub-basins is less than 50%. The degree of green water scarcity is higher than that of blue water  
443 scarcity in most of the sub-basins. Only the sub-basin 63 in downstream experienced a severe blue  
444 water scarcity.

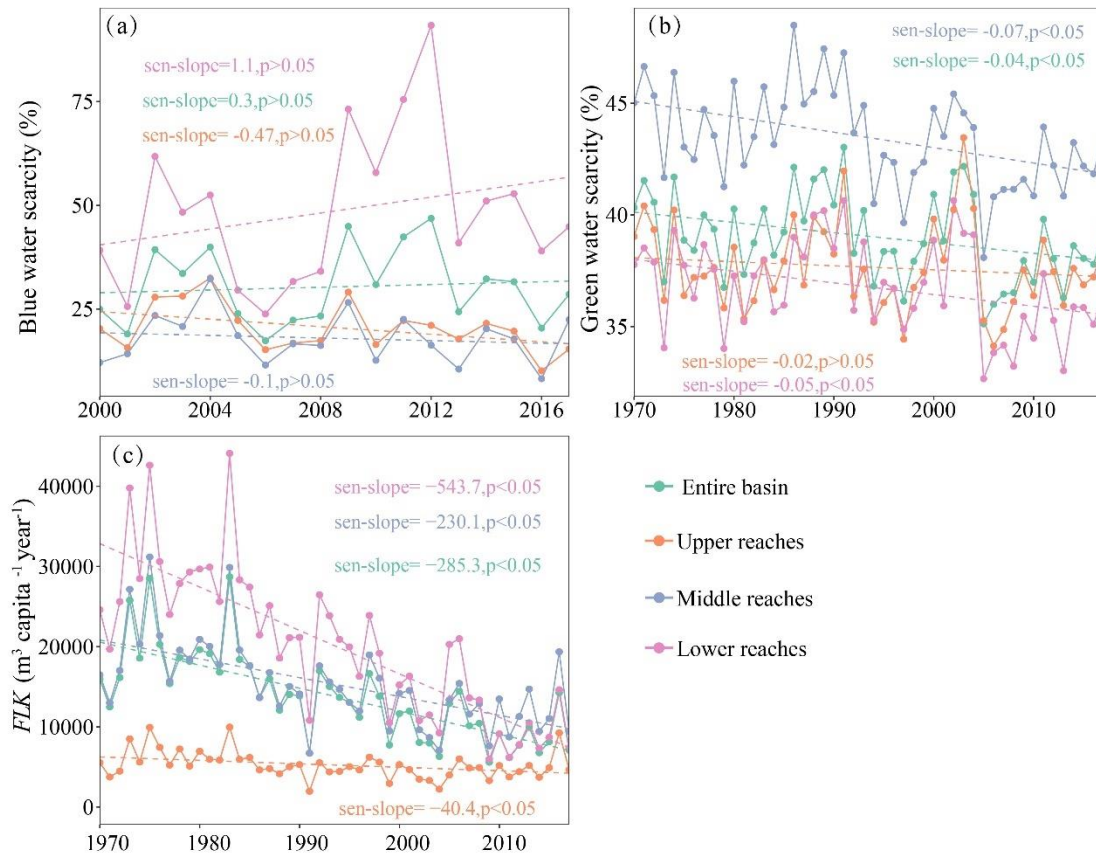


445  
446 Figure 78. Hierarchical clustering tree of (a) *BWSC*, (b) *GWSC*.

447 The interannual variations in *BWSC* and *GWSC* in DRB showed distinct regional differences.

448 *BWSC* in the basin was slowly increasing at a rate of  $0.3\% \text{ a}^{-1}$  (Fig. 8a9a). The *BWSC* in the lower  
 449 reaches slowly increased at a rate of  $1.1\% \text{ a}^{-1}$ , while the *BWSC* in the upper and middle reaches  
 450 slowly decreased at  $-0.47\% \text{ a}^{-1}$  and  $-0.1\% \text{ a}^{-1}$ , respectively. *GWSC* in the upper, middle, and lower  
 451 reaches of DRB showed a decreasing trend, with basin scale *GWSC* decreasing significantly at a  
 452 rate of  $-0.04\% \text{ a}^{-1}$  (Fig. 8b9b). Despite the acceleration of urbanization and a significant increase

453 in population in the middle and lower reaches of the watershed, blue water availability and the  
 454 amount of obtainable *BW* have been increasing. Additionally, the annual per capita water  
 455 consumption in the basin has decreased from 481.0 m<sup>3</sup> in 2000 to 245.0 m<sup>3</sup> in 2020. As a result,  
 456 the rate of increase in *BWSC* in the watershed has been relatively small. In contrast, the *GWF* in  
 457 DRB demonstrated a significant decreasing trend, and the *GWS* increased slowly. Therefore, the  
 458 *GWSC* in DRB demonstrated a significant decreasing trend. Meanwhile, the *FLK* index of the  
 459 watershed showed a significant decreasing trend (-285.3 m<sup>3</sup> per year), which means that the per  
 460 capita water resources in the watershed have significantly decreased (Fig. 8e9c). This is due to the  
 461 rapid population growth in the watershed and the slow increase in available water resources.

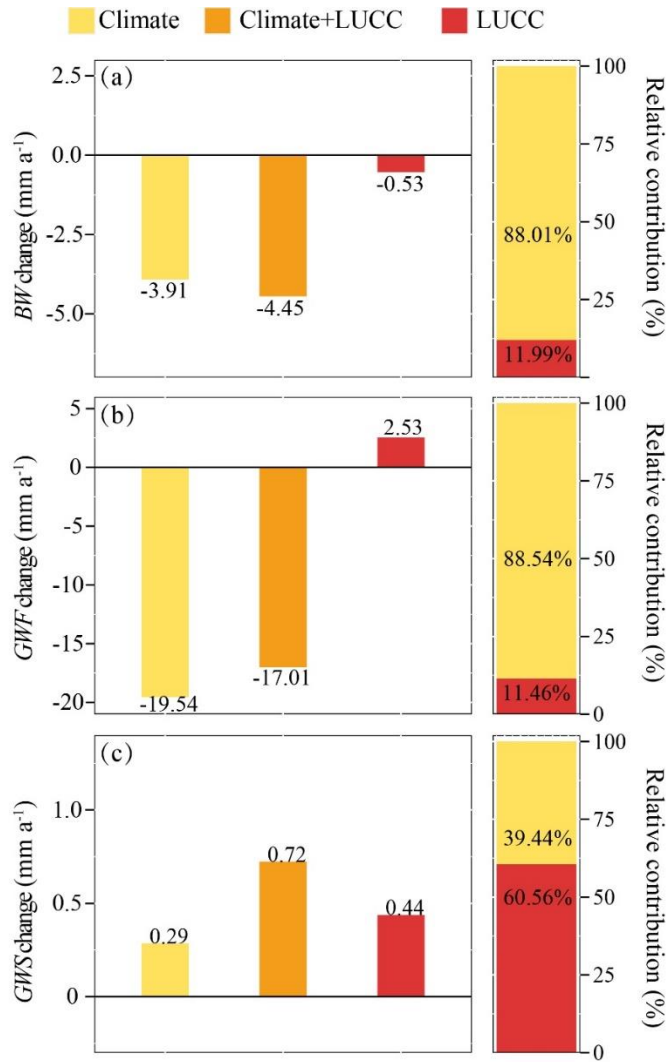


462  
 463 Figure 89. Interannual variation of (a) *BWSC*, (b) *GWSC*, and (c) *FLK* index in DRB during 1970-2017.

### 464 3.5 Impacts of LUCC and climate change on blue and green water

465 To examine the impacts of climate change and LUCC on *BW* and *GW* change, this study set  
466 three climate conditions and land use scenarios to explore this effect by comparing the scenarios  
467 (Table 3). The combined impacts of climate change and LUCC on *BW* and *GWS* in DRB were  
468 superimposed, and the combined effect on *GWF* was a negatively synergistic effect. Figure 6-10  
469 shows the variations in *BW* and *GW* under the impacts of climate change (S2-S1) and LUCC (S3-  
470 S2), as well as their combined effects (S3-S1), along with the relative contribution of climate  
471 change and LUCC to the *BW* and *GW* changes in DRB during 1970-2017. Under the joint  
472 influences of climate change and LUCC, *BW* decreased by 4.5 mm a<sup>-1</sup>. Among this decrease,  
473 climate change resulted in a loss in *BW* of 3.9 mm a<sup>-1</sup>, contributing 88.0%, while LUCC led to a  
474 loss in *BW* of 0.5 mm a<sup>-1</sup>, contributing 12.0% (Fig. 9a10a). The effect of climate change on *BW*  
475 variation is much greater than that of LUCC at the basin scale. Under the combined influences of  
476 climate change and LUCC, *GWF* decreased by 17.0 mm a<sup>-1</sup>. Among this decrease, climate change  
477 accounted for a decrease in *GWF* of 19.5 mm a<sup>-1</sup>, contributing 88.5% to the decrease, while LUCC  
478 led to an increase in *GWF* of 2.5 mm a<sup>-1</sup>, contributing 11.5% (Fig. 9b10b). Overall, the influence  
479 of climate change on *GWF* changes in the watershed is significantly more pronounced than that of  
480 LUCC. Under the joint influences of climate change and LUCC, *GWS* increased by 0.7 mm a<sup>-1</sup>.  
481 Among this increase, climate change contributed to an increase in *GWS* of 0.3 mm a<sup>-1</sup>, accounting  
482 for 39.4%, while LUCC contributed to an increase in *GWS* of 0.4 mm a<sup>-1</sup>, accounting for 60.6%

483 (Fig. 9e10c). DRB is situated in a humid region with high *GWS*, resulting in small fluctuations of  
 484 *GWS* in response to precipitation changes. The fluctuations of *GWS* are primarily influenced by  
 485 soil properties and land use. In general, the effect of climate change on the *GWS* change of DRB  
 486 is smaller than the effect of LUCC.



487  
 488 Figure 9e10. Effects and relative contribution of climate change and LUCC on the changes in (a) *BW*, (b) *GWF*,  
 489 and (c) *GWS* in DRB during 1970 to 2017.

490 Under the coupled influences of climate change and LUCC, the *BW* and *GW* resources in  
 491 DRB have changed. However, there were differences in the joint impacts of climate change and



492 LUCC on *BW* and *GW*. Both climate change and LUCC have led to the decrease of *BW* in the  
493 watershed, and the combined effect of climate change and LUCC on *BW* equals to the sum of their  
494 individual effects. Climate change, such as a decrease in potential evapotranspiration, has resulted  
495 in a decrease in *GWF* in DRB, while LUCC has led to an increase in *GWF*. Therefore, the joint  
496 impacts of climate change and LUCC on *GWF* ~~was~~were partially offset, resulting in the joint  
497 impacts of climate change and LUCC on *GWF* being less than the sum of their absolute individual  
498 effects. Both climate change and LUCC have led to an increase in *GWS* in DRB, and the joint  
499 impacts of climate change and LUCC on *GWS* equals to the sum of their individual effects.

## 500 **4 Discussion**

501 This study used the SWAT model to simulate the changes in *BW* and *GW* resources in DRB  
502 over the past five decades and their response to climate change and LUCC. It also assessed the  
503 water resource security in the basin. The findings revealed that the *GWF* exhibited a decreasing  
504 trend, and the *BW* and *GWS* exhibited an increasing trend. Liu et al. (2010) similarly found an  
505 increasing trend in annual surface runoff in DRB. Potential evapotranspiration in DRB showed a  
506 decreasing trend, which may be the main cause of the significant decrease in *GWF* in the basin  
507 (Fig. S3), and similar conclusions are obtained in He et al. (2013).

508 We show that water resources in DRB are dominated by *BW*, with a mean annual *GWI* of 0.4,  
509 which is the same as what many studies show in humid areas (Nie et al., 2023). Although the *GWI*

510 in humid areas is much smaller than that in arid areas, the ratio of *GW* in DRB still reaches 40%,  
511 so it is imperative to incorporate *GW* in the water resources assessment system. The *GWI* in the  
512 upper and middle reaches of DRB exceeded 0.4, while that in the lower reaches was only about  
513 0.3. These results mean that to ensure the appropriate utilization of water resources, effective water  
514 management in the upper and middle reaches of DRB should consider *GW* planning while water  
515 management in the lower reaches should mainly consider *BW*. The assessment results of *BWSC*  
516 and *GWSC* in DRB similarly illustrate this issue. The *GWSC* in the upper and middle reaches was  
517 bigger than that in the lower reaches of DRB, while the *BWSC* in the lower reaches of DRB was  
518 bigger than in the upper and middle reaches (Fig. 89).

519 There are robust correlations between *BW* and precipitation, *GWF* and potential  
520 evapotranspiration in DRB. Climate change plays a dominant role in variations of *BW* and *GWF*.  
521 *BW* is more sensitive to precipitation and potential evapotranspiration. *GWF* shows sensitivity to  
522 changes in potential evapotranspiration and *GWS* is influenced by both precipitation and potential  
523 evapotranspiration (Ahiablame et al., 2017; He et al., 2015). Of course, some studies in arid regions  
524 show that *GWF* is mainly affected by precipitation (Ahiablame et al., 2017), which may be linked  
525 to the hydrothermal conditions of the basin. There is sufficient precipitation in DRB, where the  
526 *GWF* changes are mainly energy-limited, and the effect of precipitation on the *GWF* is smaller.

527 Although *BW* and *GW* are mainly affected by climate change, the influences of LUCC on  
528 them cannot be ignored. The reaction of water resources to LUCC is exceedingly intricate and

529 involves various hydrological processes, including runoff yield, infiltration, and groundwater (Cuo,  
530 2016; Zhang and Shanguan, 2016). As there is a strong compensatory effect of diverse land use  
531 in the hydrological system, particularly in expansive watersheds, this could create a strong  
532 resistance to *GW* and *BW* conversion (Lin et al., 2015). A decrease in forest land or an increase in  
533 cultivated and urban land could lead to a rise in *BW* and a decline in *GW* in the watershed. Veettil  
534 and Mishra (2018) demonstrate that there is a 10% rise in forest land cover and a 1.4% drop in *BW*,  
535 indicating a negative elasticity between the two. However, the effect of urban land on streamflow  
536 in different periods showed the opposite effect. On the one hand, the increase in urban land results  
537 in increases in impermeable area and thus surface runoff in the basin, but at the same time, the  
538 increase in urban land may also reduce groundwater discharge to streamflow. At the same time,  
539 LUCC often results in changes in vegetation. Vegetation variations affect the water cycle by  
540 altering canopy interception (Shao et al., 2018; Wu et al., 2019b), transpiration (Chen et al., 2023)  
541 and canopy evaporation, and ameliorating soil structure (Qiu et al., 2022). Thus increasing  
542 vegetation often increases infiltration and soil moisture and reduces surface runoff.

543       There are several limitations and uncertainties in this research. (1) Since the quantity of the  
544 *BW* and *GW* is derived from the output results of the model simulations, including water yield, *ET*,  
545 soil moisture, and groundwater, the precision of the outcomes depends largely on the precision of  
546 the model simulations. Given the absence of observed evapotranspiration and soil moisture data  
547 for DRB, this study calibrated and validated the SWAT model using only monthly streamflow,

548 which may weaken these results to some extent. To enhance the credibility of the model, this study  
549 also utilized widely used actual evapotranspiration data (GLEAM) and soil moisture (ERA5-land)  
550 during model validation at a basin scale. The findings indicated that the simulation performance is  
551 relatively good and meets the accuracy requirements for simulation. (2) Climate change, LUCC,  
552 and large reservoir operation are the primary factors influencing the changes in hydrological  
553 conditions in DRB. The contributions of reservoir regulation, LUCC, water resource utilization,  
554 and climate change to the distribution of intra-annual flow are 33.5%, -9%, 4.5%, and 1%,  
555 respectively, during 1956-2009 (Tu et al., 2015). The operation of reservoirs, including large  
556 reservoirs like the Xinfengjiang Reservoir, is one of the important reasons for hydrological changes  
557 in DRB (Lin et al., 2014; Zhang et al., 2015). The reservoir module was not established when  
558 constructing the SWAT model in this research. To obtain natural *BW* and *GW* volumes in the  
559 watershed and mitigate the impact of hydraulic engineering, reconstructed natural streamflow  
560 based on observed flow was utilized for model calibration and validation. However, hydraulic  
561 engineering significantly influences the annual allocation of *BW*. The flow restoration considered  
562 the impacts of the three major reservoirs on the Dongjiang River and did not consider the impacts  
563 of other minor hydraulic projects and human water consumption. (3) Both the calculations of  
564 *BWSC* and the *FLK* index include environmental flows. This study represented the proportion of  
565 environmental flow in streamflow as 80%. Some studies have suggested that assuming  
566 environmental flow to be 80% of the total water resources in a basin may overestimate water

567 scarcity (Liu et al., 2017; Richter et al., 2012). Therefore, we varied the proportion of  
568 environmental flow and assessed the degree of *BWSC* using 60% and 70% proportions. Results  
569 show that only the 63rd sub-basin changed from severe *BWSC* to moderate to high *BWSC*, while  
570 other sub-basins remained with low *BWSC*. Therefore, the threshold for environmental flow has a  
571 minor impact on this paper. The assessment of *BWSC* and per capita water resources did not take  
572 into account the water demand of cities such as Shenzhen and Hong Kong, although the water  
573 supply for these cities primarily comes from the Dongjiang River through the Dongjiang-Shenzhen  
574 Water Supply Project. (4) The hydrological modeling approach utilized in this research is a  
575 frequently used method for quantitative analysis of attribution. Nevertheless, it implies  
576 independence between climate change and LUCC and does not adequately distinguish the impacts  
577 of these two components. Such restrictions ~~is~~are diffusely recognized to exist (Dey and Mishra,  
578 2017). Despite this recognized limitation, hydrological modeling methods have been widely used  
579 in numerous similar researches, yielding credible results (Li et al., 2021; Nie et al., 2023).

## 580 **5 Conclusion**

581 This study analyzed the spatio-temporal evolution of *BW* and *GW*, assessed the water security,  
582 and evaluated the effects of climate change and LUCC on *BW* and *GW* in DRB using the SWAT  
583 model. The conclusions can be outlined as follows:

584 (1) During 1970-2017, grassland, cultivated land, and forestland in DRB decreased by 4.3%,

585 10.8%, and 0.2%, respectively, while urban land and water areas increased by 137% and 2.8%,  
586 respectively. The annual precipitation and potential evapotranspiration showed a non-significant  
587 decreasing trend, while the annual average temperature showed a significantly increasing trend.

588 (2) The annual *BW*, *GWF*, and green storage in DRB from 1970-2017 were 1240.8 mm, 840.7  
589 mm, and 151.4mm, respectively. *BW* (0.14 mm a<sup>-1</sup>) and *GWS* (0.015 mm a<sup>-1</sup>) in DRB showed no  
590 significant increasing trend, and *GWF* (-0.57 mm a<sup>-1</sup>) showed a significant decreasing trend.

591 (3) The level of annual *BWSC* and *GWSC* in DRB were low, and per capita water resources  
592 exceeded 1,700 m<sup>3</sup> capita<sup>-1</sup> a<sup>-1</sup>. *BWSC* displayed a non-significant increasing trend, while the  
593 *GWSC* and *FLK* index displayed a significant decreasing trend, especially in lower reaches.

594 (4) Climate change was the major driving factor of changes in *BW* and *GWF*, and LUCC was  
595 the major driving factor of *GWS* change. Climate change contributed to 88.0%, 88.5%, and 39.4%  
596 of the changes in *BW*, *GWF*, and *GWS* in DRB, respectively. Both climate change and LUCC  
597 decrease (increase) *BW* (*GWS*), while climate change (LUCC) decreases (increases) *GWF* in DRB.

## 598 **Competing interests**

599 The contact author has declared that none of the authors has any competing interests.

## 600 **Acknowledgments**

601 This study was supported by the National Key Research and Development Program of China  
602 (2021YFC3001000), the National Natural Science Foundation of China (42401021, 52179029,

603 52179030), and the Science and Technology Program of Guangdong (NO.2024B1212040001).

## References

- Acero Triana, J. S. and Ajami, H.: Identifying Major Hydrologic Change Drivers in a Highly Managed Transboundary Endorheic Basin: Integrating Hydro-Ecological Models and Time Series Data Mining Techniques, *Water Resources Research*, 58, e2022WR032281, <https://doi.org/10.1029/2022WR032281>, 2022.
- Aghakhani Afshar, A., Hassanzadeh, Y., Pourreza-Bilondi, M., and Ahmadi, A.: Analyzing long-term spatial variability of blue and green water footprints in a semi-arid mountainous basin with MIROC-ESM model (case study: Kashafrud River Basin, Iran), *Theoretical and Applied Climatology*, 134, 885–899, <https://doi.org/10.1007/s00704-017-2309-0>, 2018.
- Ahiablame, L., Sheshukov, A. Y., Rahmani, V., and Moriasi, D.: Annual baseflow variations as influenced by climate variability and agricultural land use change in the Missouri River Basin, *Journal of Hydrology*, 551, 188–202, <https://doi.org/10.1016/j.jhydrol.2017.05.055>, 2017.
- Arnold, J. G., Srinivasan, R., Muttiah, R. S., and Williams, J. R.: Large Area Hydrologic Modeling and Assessment Part I: Model Development1, *JAWRA Journal of the American Water Resources Association*, 34, 73–89, <https://doi.org/10.1111/j.1752-1688.1998.tb05961.x>, 1998.
- Arshad, A., Mirchi, A., Samimi, M., and Ahmad, B.: Combining downscaled-GRACE data with SWAT to improve the estimation of groundwater storage and depletion variations in the Irrigated Indus Basin (IIB), *Science of The Total Environment*, 838, 156044, <https://doi.org/10.1016/j.scitotenv.2022.156044>, 2022.
- Bai, P., Liu, X., Zhang, Y., and Liu, C.: Assessing the Impacts of Vegetation Greenness Change on Evapotranspiration and Water Yield in China, *Water Resour. Res.*, 56, <https://doi.org/10.1029/2019WR027019>, 2020.
- Berezovskaya, S., Yang, D., and Kane, D. L.: Compatibility analysis of precipitation and runoff trends over the large Siberian watersheds, *Geophysical Research Letters*, 31, <https://doi.org/10.1029/2004GL021277>, 2004.
- Chagas, V. B. P., Chaffe, P. L. B., and Blöschl, G.: Climate and land management accelerate the Brazilian water cycle, *Nat Commun*, 13, 5136, <https://doi.org/10.1038/s41467-022-32580-x>, 2022.
- Chen, Z., Wang, W., Cescatti, A., and Forzieri, G.: Climate-driven vegetation greening further reduces water availability in drylands, *Global Change Biology*, 29, 1628–1647, <https://doi.org/10.1111/gcb.16561>, 2023.
- Chouchane, H., Krol, M. S., and Hoekstra, A. Y.: Changing global cropping patterns to minimize national blue water scarcity, *Hydrology and Earth System Sciences*, 24, 3015–3031, <https://doi.org/10.5194/hess-24-3015-2020>, 2020.
- Cook, B. I., Smerdon, J. E., Seager, R., and Coats, S.: Global warming and 21 st century drying, *Climate Dynamics*, 43, 2607–2627, <https://doi.org/10.1007/s00382-014-2075-y>, 2014.
- Cooper, C. M., Troutman, J. P., Awal, R., Habibi, H., and Fares, A.: Climate change-induced



- variations in blue and green water usage in U.S. urban agriculture, *Journal of Cleaner Production*, 348, 131326, <https://doi.org/10.1016/j.jclepro.2022.131326>, 2022.
- Cuo, L.: Land use/cover change impacts on hydrology in large river basins: a review, *Terrestrial Water Cycle and Climate Change: Natural and Human-Induced Impacts*, 221, 103, <https://doi.org/10.1002/9781118971772.ch6>, 2016.
- Dai, C., Qin, X., Dong, F., and Cai, Y.: Climate change impact on blue and green water resources distributions in the Beijiang River basin based on CORDEX projections, *Journal of Water and Climate Change*, 13, 2780–2798, <https://doi.org/10.2166/wcc.2022.115>, 2022.
- Dey, P. and Mishra, A.: Separating the impacts of climate change and human activities on streamflow: A review of methodologies and critical assumptions, *Journal of Hydrology*, 548, 278–290, <https://doi.org/10.1016/j.jhydrol.2017.03.014>, 2017.
- Ding, B., Zhang, J., Zheng, P., Li, Z., Wang, Y., Jia, G., and Yu, X.: Water security assessment for effective water resource management based on multi-temporal blue and green water footprints, *Journal of Hydrology*, 632, 130761, <https://doi.org/10.1016/j.jhydrol.2024.130761>, 2024.
- Eekhout, J. P. C., Hunink, J. E., Terink, W., and de Vente, J.: Why increased extreme precipitation under climate change negatively affects water security, *Hydrology and Earth System Sciences*, 22, 5935–5946, <https://doi.org/10.5194/hess-22-5935-2018>, 2018.
- Falkenmark, M. and Rockström, J.: The New Blue and Green Water Paradigm: Breaking New Ground for Water Resources Planning and Management, *Journal of Water Resources Planning and Management*, 132, 129–132, [https://doi.org/10.1061/\(ASCE\)0733-9496\(2006\)132:3\(129\)](https://doi.org/10.1061/(ASCE)0733-9496(2006)132:3(129)), 2006.
- Falkenmark, M., Lundqvist, J., and Widstrand, C.: Macro-scale water scarcity requires micro-scale approaches, *Natural Resources Forum*, 13, 258–267, <https://doi.org/10.1111/j.1477-8947.1989.tb00348.x>, 1989.
- Falkenmark, M., Folke, C., and Falkenmark, M.: Freshwater as shared between society and ecosystems: from divided approaches to integrated challenges, *Philosophical Transactions of the Royal Society of London. Series B: Biological Sciences*, 358, 2037–2049, <https://doi.org/10.1098/rstb.2003.1386>, 2003.
- Ficklin, D. L., Robeson, S. M., and Knouft, J. H.: Impacts of recent climate change on trends in baseflow and stormflow in United States watersheds, *Geophys Res Lett*, 43, 5079–5088, <https://doi.org/10.1002/2016gl069121>, 2016.
- Fischer, G., Nachtergaele, F., Prieler, S., Van Velthuisen, H. T., Verelst, L., and Wiberg, D.: Global agro-ecological zones assessment for agriculture (GAEZ 2008), IIASA, Laxenburg, Austria and FAO, Rome, Italy, 10, 2008.
- Foley, J. A., DeFries, R., Asner, G. P., Barford, C., Bonan, G., Carpenter, S. R., Chapin, F. S., Coe, M. T., Daily, G. C., and Gibbs, H. K.: Global consequences of land use, *Science*, 309, 570–574, <https://doi.org/10.1126/science.1111772>, 2005.
- Han, Z., Huang, S., Huang, Q., Bai, Q., Leng, G., Wang, H., Zhao, J., Wei, X., and Zheng, X.: Effects of vegetation restoration on groundwater drought in the Loess Plateau, China, *Journal of Hydrology*, 591, 125566, <https://doi.org/10.1016/j.jhydrol.2020.125566>, 2020.

- He, Y., Lin, K., and Chen, X.: Effect of Land Use and Climate Change on Runoff in the Dongjiang Basin of South China, *Mathematical Problems in Engineering*, 2013, e471429, <https://doi.org/10.1155/2013/471429>, 2013.
- He, Y., Lin, K., Chen, X., Ye, C., and Cheng, L.: Classification-Based Spatiotemporal Variations of Pan Evaporation Across the Guangdong Province, South China, *Water Resour Manage*, 29, 901–912, <https://doi.org/10.1007/s11269-014-0850-5>, 2015.
- Hoek van Dijke, A. J., Herold, M., Mallick, K., Benedict, I., Machwitz, M., Schlerf, M., Pranindita, A., Theeuwens, J. J. E., Bastin, J.-F., and Teuling, A. J.: Shifts in regional water availability due to global tree restoration, *Nature Geoscience*, 15, 363–368, <https://doi.org/10.1038/s41561-022-00935-0>, 2022.
- Hoekstra, A. Y., Mekonnen, M. M., Chapagain, A. K., Mathews, R. E., and Richter, B. D.: Global Monthly Water Scarcity: Blue Water Footprints versus Blue Water Availability, *PLOS ONE*, 7, e32688, <https://doi.org/10.1371/journal.pone.0032688>, 2012.
- Honrado, J. P., Vieira, C., Soares, C., Monteiro, M. B., Marcos, B., Pereira, H. M., and Partidário, M. R.: Can we infer about ecosystem services from EIA and SEA practice? A framework for analysis and examples from Portugal, *Environmental Impact Assessment Review*, 40, 14–24, <https://doi.org/10.1016/j.eiar.2012.12.002>, 2013.
- Hordofa, A. T., Leta, O. T., Alamirew, T., and Chukalla, A. D.: Climate Change Impacts on Blue and Green Water of Meki River Sub-Basin, *Water Resour Manage*, 37, 2835–2851, <https://doi.org/10.1007/s11269-023-03490-4>, 2023.
- Huang, H., Xue, Y., Chilukoti, N., Liu, Y., Chen, G., and Diallo, I.: Assessing Global and Regional Effects of Reconstructed Land-Use and Land-Cover Change on Climate since 1950 Using a Coupled Land–Atmosphere–Ocean Model, *Journal of Climate*, 33, 8997–9013, <https://doi.org/10.1175/JCLI-D-20-0108.1>, 2020.
- Huang, Y., Cai, Y., Xie, Y., Zhang, F., He, Y., Zhang, P., Li, B., Li, B., Jia, Q., Wang, Y., and Qi, Z.: An optimization model for water resources allocation in Dongjiang River Basin of Guangdong-Hong Kong-Macao Greater Bay Area under multiple complexities, *Science of The Total Environment*, 820, 153198, <https://doi.org/10.1016/j.scitotenv.2022.153198>, 2022.
- Jiang, J., Wang, Z., Lai, C., Wu, X., and Chen, X.: Climate and landuse change enhance spatio-temporal variability of Dongjiang river flow and ammonia nitrogen, *Science of The Total Environment*, 867, 161483, <https://doi.org/10.1016/j.scitotenv.2023.161483>, 2023.
- Konapala, G., Mishra, A. K., Wada, Y., and Mann, M. E.: Climate change will affect global water availability through compounding changes in seasonal precipitation and evaporation, *Nat Commun*, 11, 3044, <https://doi.org/10.1038/s41467-020-16757-w>, 2020.
- Lee, X., Goulden, M. L., Hollinger, D. Y., Barr, A., Black, T. A., Bohrer, G., Bracho, R., Drake, B., Goldstein, A., and Gu, L.: Observed increase in local cooling effect of deforestation at higher latitudes, *Nature*, 479, 384–387, <https://doi.org/10.1038/nature10588>, 2011.
- Li, C., Tang, G., and Hong, Y.: Cross-evaluation of ground-based, multi-satellite and reanalysis precipitation products: Applicability of the Triple Collocation method across Mainland China, *Journal of Hydrology*, 562, 71–83, <https://doi.org/10.1016/j.jhydrol.2018.04.039>, 2018.
- Li, X., Zhang, Y., Ma, N., Li, C., and Luan, J.: Contrasting effects of climate and LULC change

- on blue water resources at varying temporal and spatial scales, *Science of The Total Environment*, 786, 147488, <https://doi.org/10.1016/j.scitotenv.2021.147488>, 2021.
- Lian, X., Piao, S., Li, L. Z. X., Li, Y., Huntingford, C., Ciais, P., Cescatti, A., Janssens, I. A., Peñuelas, J., Buermann, W., Chen, A., Li, X., Myneni, R. B., Wang, X., Wang, Y., Yang, Y., Zeng, Z., Zhang, Y., and McVicar, T. R.: Summer soil drying exacerbated by earlier spring greening of northern vegetation, *Science Advances*, 6, eaax0255, <https://doi.org/10.1126/sciadv.aax0255>, 2020.
- Liang, J., He, X., Zeng, G., Zhong, M., Gao, X., Li, X., Li, X., Wu, H., Feng, C., and Xing, W.: Integrating priority areas and ecological corridors into national network for conservation planning in China, *Science of the Total Environment*, 626, 22–29, <https://doi.org/10.1016/j.scitotenv.2018.01.086>, 2018.
- Liang, J., Liu, Q., Zhang, H., Li, X., Qian, Z., Lei, M., Li, X., Peng, Y., Li, S., and Zeng, G.: Interactive effects of climate variability and human activities on blue and green water scarcity in rapidly developing watershed, *Journal of Cleaner Production*, 265, 121834, <https://doi.org/10.1016/j.jclepro.2020.121834>, 2020.
- Lin, B., Chen, X., Yao, H., Chen, Y., Liu, M., Gao, L., and James, A.: Analyses of landuse change impacts on catchment runoff using different time indicators based on SWAT model, *Ecological Indicators*, 58, 55–63, <https://doi.org/10.1016/j.ecolind.2015.05.031>, 2015.
- Lin, K., Lian, Y., Chen, X., and Lu, F.: Changes in runoff and eco-flow in the Dongjiang River of the Pearl River Basin, China, *Front. Earth Sci.*, 8, 547–557, <https://doi.org/10.1007/s11707-014-0434-y>, 2014.
- Liu, B., Peng, S., Liao, Y., and Long, W.: The causes and impacts of water resources crises in the Pearl River Delta, *Journal of Cleaner Production*, 177, 413–425, <https://doi.org/10.1016/j.jclepro.2017.12.203>, 2018.
- Liu, D., Chen, X., Lian, Y., and Lou, Z.: Impacts of climate change and human activities on surface runoff in the Dongjiang River basin of China, *Hydrological Processes*, 24, 1487–1495, <https://doi.org/10.1002/hyp.7609>, 2010.
- Liu, J., Yang, H., Gosling, S. N., Kummu, M., Flörke, M., Pfister, S., Hanasaki, N., Wada, Y., Zhang, X., Zheng, C., Alcamo, J., and Oki, T.: Water scarcity assessments in the past, present, and future, *Earth's Future*, 5, 545–559, <https://doi.org/10.1002/2016EF000518>, 2017.
- Liu, M., Wang, D., Chen, X., Chen, Y., Gao, L., and Deng, H.: Impacts of climate variability and land use on the blue and green water resources in a subtropical basin of China, *Sci Rep*, 12, 20993, <https://doi.org/10.1038/s41598-022-21880-3>, 2022.
- Liu, M., Zhang, P., Cai, Y., Chu, J., Li, Y., Wang, X., Li, C., and Liu, Q.: Spatial-temporal heterogeneity analysis of blue and green water resources for Poyang Lake basin, China, *Journal of Hydrology*, 617, 128983, <https://doi.org/10.1016/j.jhydrol.2022.128983>, 2023.
- Martens, B., Miralles, D. G., Lievens, H., Fernández-Prieto, D., Beck, H. E., Dorigo, W. A., and Verhoest, N. E. C.: GLEAM v3: satellite-based land evaporation and root-zone soil moisture, *Geoscientific Model Development*, 10, 1903–1925, <https://doi.org/10.5194/gmd-10-1903-2017>, 2017.
- Martínez-Salvador, A. and Conesa-García, C.: Suitability of the SWAT Model for Simulating

- Water Discharge and Sediment Load in a Karst Watershed of the Semiarid Mediterranean Basin, *Water Resour Manage*, 34, 785–802, <https://doi.org/10.1007/s11269-019-02477-4>, 2020.
- Mohan, M. and Kandya, A.: Impact of urbanization and land-use/land-cover change on diurnal temperature range: A case study of tropical urban airshed of India using remote sensing data, *Science of the Total Environment*, 506, 453–465, <https://doi.org/10.1016/j.scitotenv.2014.11.006>, 2015.
- Muñoz Sabater, J.: ERA5-Land monthly averaged data from 1981 to present, Copernicus Climate Change Service (C3S) Climate Data Store (CDS), 2019.
- Nearing, M. A., Jetten, V., Baffaut, C., Cerdan, O., Couturier, A., Hernandez, M., Le Bissonnais, Y., Nichols, M. H., Nunes, J. P., and Renschler, C. S.: Modeling response of soil erosion and runoff to changes in precipitation and cover, *CATENA*, 61, 131–154, <https://doi.org/10.1016/j.catena.2005.03.007>, 2005.
- Neitsch, S., Arnold, J., Kiniry, J., Williams, J., and King, K.: Soil and water assessment tool (SWAT): theoretical documentation, version 2000, Texas Water Resources Institute, College Station, Texas, TWRI Report TR-191, 2002.
- Nie, N., Li, T., Miao, Y., Zhang, W., Gao, H., He, H., Zhao, D., and Liu, M.: Asymmetry of blue and green water changes in the Yangtze river basin, China, examined by multi-water-variable calibrated SWAT model, *Journal of Hydrology*, 625, 130099, <https://doi.org/10.1016/j.jhydrol.2023.130099>, 2023.
- Pandey, B. K., Khare, D., Kawasaki, A., and Mishra, P. K.: Climate Change Impact Assessment on Blue and Green Water by Coupling of Representative CMIP5 Climate Models with Physical Based Hydrological Model, *Water Resour Manage*, 33, 141–158, <https://doi.org/10.1007/s11269-018-2093-3>, 2019.
- Pokhrel, Y., Felfelani, F., Satoh, Y., Boulange, J., Burek, P., Gädeke, A., Gerten, D., Gosling, S. N., Grillakis, M., Gudmundsson, L., Hanasaki, N., Kim, H., Koutroulis, A., Liu, J., Papadimitriou, L., Schewe, J., Müller Schmied, H., Stacke, T., Telteu, C.-E., Thiery, W., Veldkamp, T., Zhao, F., and Wada, Y.: Global terrestrial water storage and drought severity under climate change, *Nat. Clim. Chang.*, 11, 226–233, <https://doi.org/10.1038/s41558-020-00972-w>, 2021.
- Qiu, D., Xu, R., Wu, C., Mu, X., Zhao, G., and Gao, P.: Vegetation restoration improves soil hydrological properties by regulating soil physicochemical properties in the Loess Plateau, China, *Journal of Hydrology*, 609, 127730, <https://doi.org/10.1016/j.jhydrol.2022.127730>, 2022.
- Qiu, D., Xu, R., Wu, C., Mu, X., Zhao, G., and Gao, P.: Effects of vegetation restoration on soil infiltrability and preferential flow in hilly gully areas of the Loess Plateau, China, *CATENA*, 221, 106770, <https://doi.org/10.1016/j.catena.2022.106770>, 2023.
- Richter, B. D.: Re-thinking environmental flows: from allocations and reserves to sustainability boundaries, *River Research and Applications*, 26, 1052–1063, <https://doi.org/10.1002/rra.1320>, 2010.
- Richter, B. D., Davis, M. M., Apse, C., and Konrad, C.: A Presumptive Standard for Environmental Flow Protection, *River Research and Applications*, 28, 1312–1321,

- <https://doi.org/10.1002/rra.1511>, 2012.
- Schewe, J., Heinke, J., Gerten, D., Haddeland, I., Arnell, N. W., Clark, D. B., Dankers, R., Eisner, S., Fekete, B. M., Colón-González, F. J., Gosling, S. N., Kim, H., Liu, X., Masaki, Y., Portmann, F. T., Satoh, Y., Stacke, T., Tang, Q., Wada, Y., Wisser, D., Albrecht, T., Frieler, K., Piontek, F., Warszawski, L., and Kabat, P.: Multimodel assessment of water scarcity under climate change, *Proceedings of the National Academy of Sciences*, 111, 3245–3250, <https://doi.org/10.1073/pnas.1222460110>, 2014.
- Schuol, J., Abbaspour, K. C., Yang, H., Srinivasan, R., and Zehnder, A. J.: Modeling blue and green water availability in Africa, *Water resources research*, 44, <https://doi.org/10.1029/2007WR006609>, 2008.
- Schyns, J. F., Hoekstra, A. Y., Booij, M. J., Hogeboom, R. J., and Mekonnen, M. M.: Limits to the world's green water resources for food, feed, fiber, timber, and bioenergy, *Proceedings of the National Academy of Sciences*, 116, 4893–4898, <https://doi.org/10.1073/pnas.1817380116>, 2019.
- Shao, M., Wang, Y., Xia, Y., and Jia, X.: Soil drought and water carrying capacity for vegetation in the critical zone of the Loess Plateau: A review, *Vadose Zone Journal*, 17, 1539–1663, <https://doi.org/10.2136/vzj2017.04.0077>, 2018.
- Sharma, A., Patel, P. L., and Sharma, P. J.: Blue and green water accounting for climate change adaptation in a water scarce river basin, *Journal of Cleaner Production*, 426, 139206, <https://doi.org/10.1016/j.jclepro.2023.139206>, 2023.
- Shen, Q., Cong, Z., and Lei, H.: Evaluating the impact of climate and underlying surface change on runoff within the Budyko framework: A study across 224 catchments in China, *Journal of Hydrology*, 554, 251–262, <https://doi.org/10.1016/j.jhydrol.2017.09.023>, 2017.
- Stocker, B. D., Tumber-Dávila, S. J., Konings, A. G., Anderson, M. C., Hain, C., and Jackson, R. B.: Global patterns of water storage in the rooting zones of vegetation, *Nat. Geosci.*, 1–7, <https://doi.org/10.1038/s41561-023-01125-2>, 2023.
- Suzuki, K., Park, H., Makarieva, O., Kanamori, H., Hori, M., Matsuo, K., Matsumura, S., Nesterova, N., and Hiyama, T.: Effect of Permafrost Thawing on Discharge of the Kolyma River, Northeastern Siberia, *Remote Sensing*, 13, 4389, <https://doi.org/10.3390/rs13214389>, 2021.
- Tan, X., Liu, B., and Tan, X.: Global Changes in Baseflow Under the Impacts of Changing Climate and Vegetation, *Water Resources Research*, 56, e2020WR027349, <https://doi.org/10.1029/2020WR027349>, 2020.
- Tan, X., Wu, X., Huang, Z., Deng, S., Hu, M., and Yew Gan, T.: Detection and attribution of the decreasing precipitation and extreme drought 2020 in southeastern China, *Journal of Hydrology*, 610, 127996, <https://doi.org/10.1016/j.jhydrol.2022.127996>, 2022a.
- Tan, X., Liu, B., Tan, X., and Chen, X.: Long-Term Water Imbalances of Watersheds Resulting From Biases in Hydroclimatic Data Sets for Water Budget Analyses, *Water Resources Research*, 58, e2021WR031209, <https://doi.org/10.1029/2021WR031209>, 2022b.
- Tan, X., Tan, X., Liu, B., and Huang, Z.: Contribution of changes in vegetation composition and climate variability on streamflow across the global watersheds, *CATENA*, 232, 107394,

- <https://doi.org/10.1016/j.catena.2023.107394>, 2023.
- Tao, S., Fang, J., Ma, S., Cai, Q., Xiong, X., Tian, D., Zhao, X., Fang, L., Zhang, H., Zhu, J., and Zhao, S.: Changes in China's lakes: climate and human impacts, *National Science Review*, 7, 132–140, <https://doi.org/10.1093/nsr/nwz103>, 2020.
- Tu, X., Singh, V. P., Chen, X., Chen, L., Zhang, Q., and Zhao, Y.: Intra-annual Distribution of Streamflow and Individual Impacts of Climate Change and Human Activities in the Dongjiang River Basin, China, *Water Resour Manage*, 29, 2677–2695, <https://doi.org/10.1007/s11269-015-0963-5>, 2015.
- Tu, X., Wu, H., Singh, V. P., Chen, X., Lin, K., and Xie, Y.: Multivariate design of socioeconomic drought and impact of water reservoirs, *Journal of Hydrology*, 566, 192–204, <https://doi.org/10.1016/j.jhydrol.2018.09.012>, 2018.
- Vano, J. A., Das, T., and Lettenmaier, D. P.: Hydrologic sensitivities of Colorado River runoff to changes in precipitation and temperature, *Journal of Hydrometeorology*, 13, 932–949, <https://doi.org/10.1175/JHM-D-11-069.1>, 2012.
- Veetil, A. V. and Mishra, A.: Water Security Assessment for the Contiguous United States Using Water Footprint Concepts, *Geophysical Research Letters*, 47, e2020GL087061, <https://doi.org/10.1029/2020GL087061>, 2020.
- Veetil, A. V. and Mishra, A. K.: Water security assessment using blue and green water footprint concepts, *Journal of Hydrology*, 542, 589–602, <https://doi.org/10.1016/j.jhydrol.2016.09.032>, 2016.
- Veetil, A. V. and Mishra, A. K.: Potential influence of climate and anthropogenic variables on water security using blue and green water scarcity, Falkenmark index, and freshwater provision indicator, *Journal of Environmental Management*, 228, 346–362, <https://doi.org/10.1016/j.jenvman.2018.09.012>, 2018.
- Walters, K. M. and Babbar-Sebens, M.: Using climate change scenarios to evaluate future effectiveness of potential wetlands in mitigating high flows in a Midwestern US watershed, *Ecological engineering*, 89, 80–102, <https://doi.org/10.1016/j.ecoleng.2016.01.014>, 2016.
- Wu, J., Chen, X., Yu, Z., Yao, H., Li, W., and Zhang, D.: Assessing the impact of human regulations on hydrological drought development and recovery based on a ‘simulated-observed’ comparison of the SWAT model, *Journal of Hydrology*, 577, 123990, <https://doi.org/10.1016/j.jhydrol.2019.123990>, 2019a.
- Wu, J., Liu, L., Sun, C., Su, Y., Wang, C., Yang, J., Liao, J., He, X., Li, Q., Zhang, C., and Zhang, H.: Estimating Rainfall Interception of Vegetation Canopy from MODIS Imageries in Southern China, *Remote Sensing*, 11, 2468, <https://doi.org/10.3390/rs11212468>, 2019b.
- Wu, J., Chen, X., Yuan, X., Yao, H., Zhao, Y., and AghaKouchak, A.: The interactions between hydrological drought evolution and precipitation-streamflow relationship, *Journal of Hydrology*, 597, 126210, <https://doi.org/10.1016/j.jhydrol.2021.126210>, 2021.
- Xu, X.: China population spatial distribution kilometer grid dataset, Data Registration and Publishing System of Resource and Environmental Science Data Center of Chinese Academy of Sciences, 2017.
- Xu, X., Liu, J., Zhang, S., Li, R., Yan, C., and Wu, S.: Multi-period land use land cover remote

- sensing monitoring dataset in China (CNLUCC), Resource and Environmental Science Data Registration and Publication System. (<http://www.resdc.cn/DOI>), <https://doi.org/DOI:10.12078/2018070201>, 2018.
- Yang, L. E., Chan, F. K. S., and Scheffran, J.: Climate change, water management and stakeholder analysis in the Dongjiang River basin in South China, *International Journal of Water Resources Development*, 34, 166–191, <https://doi.org/10.1080/07900627.2016.1264294>, 2018.
- Zang, C. and Liu, J.: Trend analysis for the flows of green and blue water in the Heihe River basin, northwestern China, *Journal of Hydrology*, 502, 27–36, <https://doi.org/10.1016/j.jhydrol.2013.08.022>, 2013.
- Zhang, Q., Gu, X., Singh, V. P., and Chen, X.: Evaluation of ecological instream flow using multiple ecological indicators with consideration of hydrological alterations, *Journal of Hydrology*, 529, 711–722, <https://doi.org/10.1016/j.jhydrol.2015.08.066>, 2015.
- Zhang, Y. and Shangguan, Z.: The change of soil water storage in three land use types after 10 years on the Loess Plateau, *CATENA*, 147, 87–95, <https://doi.org/10.1016/j.catena.2016.06.036>, 2016.
- Zhang, Y., Xia, J., Yu, J., Randall, M., Zhang, Y., Zhao, T., Pan, X., Zhai, X., and Shao, Q.: Simulation and assessment of urbanization impacts on runoff metrics: insights from land use changes, *Journal of Hydrology*, 560, 247–258, <https://doi.org/10.1016/j.jhydrol.2018.03.031>, 2018.
- Zuo, D., Xu, Z., Peng, D., Song, J., Cheng, L., Wei, S., Abbaspour, K. C., and Yang, H.: Simulating spatiotemporal variability of blue and green water resources availability with uncertainty analysis, *Hydrological Processes*, 29, 1942–1955, <https://doi.org/10.1002/hyp.10307>, 2015.